Mapping classes associated to mixed-sign Coxeter graphs

Eriko Hironaka*

December 17, 2013

Abstract

In this paper, we define and study properties of generalized Coxeter mapping classes on surfaces. Like the mapping classes associated to classical Coxeter graphs studied by Thurston and Leininger, the action on first homology is conjugate to the action of the Coxeter element of the associated Coxeter system considered as a reflection group, making classification and computations of invariants easier. However, unlike in the classical case, where dilatations of pseudo-Anosov examples are bounded from below by Lehmer's number, the generalized Coxeter graphs may be used to construct pseudo-Anosov mapping classes with dilatation arbitrarily close to one. We observe that the smallest dilatation orientable pseudo-Anosov mapping classes of genus 2,3,4 and 5 found by Lanneau and Thiffeault can be realized as generalized Coxeter mapping classes, and that the smallest known accumulation point of normalized dilatations can be realized as the limit of normalized dilatations of a sequence of generalized Coxeter mapping classes. For the latter construction, we define non-classical periodic Coxeter mapping classes and use them as building blocks to define *twisted mapping classes*. We give sufficient conditions so that a sequence of twisted mapping classes corresponds to a convergent sequence on a fibered face.

1 Introduction

Let S be a compact oriented surface of finite type. A mapping class on S is an isotopy class of self-homeomorphisms of S. Of particular interest are the *irreducible* mapping classes, which do not fix any nontrivial multi-curves on S. Such mapping classes ϕ are called *pseudo-Anosov* and have the property that for some pair of ϕ-invariant, singular foliations $\mathcal{F}^+$ and $\mathcal{F}^-$, with transverse measures ν^+ and ν^-, we have $\nu^{\pm}(\phi(x),\phi(y)) = \lambda^{\pm 1}(x,y)$, for x and y points on the nonsingular locus of $\mathcal{F}^{\pm}$ ([38], [13]). When the leaves in $\mathcal{F}^{\pm}$ can be given a consistent orientation, we say that ϕ is an *orientable pseudo-Anosov mapping class*. This is equivalent to the statement that the dilatation $\lambda(\phi)$ equals the homological dilatation of ϕ, that is, the spectral radius of the action of ϕ on the first homology of S. The minimum possible value of $\lambda(\phi)$ for a fixed surface S is known only for surfaces with small genus and number of boundary components [23] [15] [9] [26]. Slightly more is known for the case of orientable pseudo-Anosov mapping classes [18] [25].

*This work was partially supported by a grant from the Simons Foundation (#209171 to Eriko Hironaka).

The minimum dilatation of pseudo-Anosov mapping classes on a surface S is known to go to 1 as the absolute value of the topological Euler characteristic $|\chi(S)|$ goes to infinity. The first proof of this was given in [31], and the orientable case was shown in [18]. The minimum value of $L(S,\phi)$ for $S = S_{g,n}$ is bounded for (g,n) on any line of rational slope through the origin [31] [18] [39] [41], but unbounded on any line with g constant: $g = g_0 \geq 2$ [39]. We will say that a pseudo-Anosov mapping class has *small dilatation* if the *normalized dilatation*

$$L(S,\phi) = \lambda(\phi)^{|\chi(S)|}$$

is small.

Question 1.1 *What do small dilatation pseudo-Anosov mapping classes look like?*

In this paper, we approach question 1.1 by studying a simple construction of pseudo-Anosov mapping classes from generalized Coxeter graphs. We call such mapping classes *mixed-sign Coxeter mapping classes*. Our main result is the following.

Theorem 1.2 *The set of normalized dilatations of pseudo-Anosov mixed-sign Coxeter mapping classes has accumulation point γ_0^4.*

The minimum accumulation point ℓ_0 of $L(S,\phi)$ over all pseudo-Anosov mapping classes satisfies

$$2 < \ell_0 \leq \left(\frac{3+\sqrt{5}}{2}\right)^2 = \gamma_0^4 \approx 6.8541, \tag{1}$$

where γ_0 is the golden mean ([17] [1] [22]). The lower bound comes from properties of directed graphs (see [31] [28]). The upper bound γ_0^4 in (1) is achieved by the *simplest hyperbolic braid* (see, for example, [28] [17]). Smaller normalized dilatations exist, for example, for the once-punctured torus, the smallest normalized dilatation is $\frac{3+\sqrt{5}}{2} \approx 2.61803$, and the smallest normalized dilatation for a closed genus 2 surface $|x^4 - 2x^2 - 2x + 1| \approx 5.27451$.

1.1 Fibered face theory

By Thurston's fibered face theory [37] and a result of Fried [14], the rational points on fibered faces of hyperbolic 3-manifolds parameterize all pseudo-Anosov mapping classes on compact oriented surfaces (this is explained in more detail below. Since the simplest hyperbolic braid has normalized dilatation equal to γ_0^4, and its fibered face has positive dimension, the values of L are dense in the interval $[\gamma_0^4, \infty)$ (see [17]). The genus 1 and genus 2 examples mentioned above lie on fibered faces consisting of a single point, and can be considered as isolated points in the space of pseudo-Anosov mapping classes.

The Universal Finiteness Theorem of Farb, Leininger and Marglit [11] implies that there is a finite collection of mapping tori (up to homeomorphism) for pseudo-Anosov mapping classes with no

interior singularities whose normalized dilatations is bounded. Fibered face theory implies that the dynamical structure of small dilatation mapping classes are governed by a finite set of "templates" defined by pseudo-Anosov flows on hyperbolic 3-manifolds [37] [14] [11].

More precisely, if a hyperbolic 3-manifold M is fibered and has first Betti number $b_1(M)$ greater than or equal to 2, then there is at least one open cone, called a *fibered cone*, in $\mathbb{R}^{b_1(M)}$ whose primitive integral points parameterize fibrations of M to S^1. This fibered cone is of the form $F \cdot \mathbb{R}^+$, where F is a fibered face of the Thurston norm ball for M in $H^1(M;\mathbb{R})$ (see [37] and Section 3.3 for definitions). By a result of Fried [14] the normalized dilatation function L extends to a continuous convex function on the cone $F \cdot \mathbb{R}^+$ so that $\log L$ is homogeneous of degree -1. It follows that on every compact subset of F there are pseudo-Anosov mapping classes with unbounded topological Euler characteristic and bounded normalized dilatation. Conversely, if we restrict to pseudo-Anosov mapping classes with no interior singularities, all such infinite families lie on a finite union of such fibered faces by the Universal Finiteness Theorem. Thus, Question 1.1 is strongly connected to the question.

Question 1.3 *What do mapping classes associated to rational points on a single fibered face look like?*

So far there has been no explicit characterization of which 3-manifolds realize minimum normalized diatations smaller than a given bound, nor has there been a simple constructive description of the infinite family of pseudo-Anosov maps associated to the rational points on an arbitrary fibered face.

Our main new technique in this paper is to show that there are natural sequences of mapping classes associated to generalized Coxeter graphs that correspond to Cauchy sequences on fibered faces. We show that generalized Coxeter mapping classes contain a large family of periodic mapping classes on surfaces with high symmetry. These provide useful building blocks for defining small dilatation pseudo-Anosov mapping classes. We observe that the minimum dilatation orientable pseudo-Anosov mapping classes for genus $g = 2, 3, 4, 5$ found by Lanneau and Thiffeault [25] can be defined from generalized Coxeter graphs (Table 2.6). We also define a sequence (S_n, ϕ_n) of pseudo-Anosov mapping classes whose normalized dilatations converge to γ_0^4 (Section 3.8).

1.2 Mixed-sign Coxeter reflection groups.

A mixed-sign Coxeter system is a generalization of classical Coxeter systems. A *(simply-laced, classical) Coxeter graph* is a finite connected graph with no self- or double-edges. A Coxeter graph Γ defines a *Coxeter reflection group* $\mathcal{W}_\Gamma \subset \mathrm{GL}(\mathbb{R}^\mathcal{V})$, where $\mathcal{V}$ is the set of vertices of Γ, and $\mathbb{R}^\mathcal{V}$ is the vector space of $\mathbb{R}$ valued functions on $\mathcal{V}$. The group $\mathcal{W}_\Gamma$ is generated by a distinguished set of reflections $S = \{s_1, \ldots, s_k\}$ preserving the bilinear form $B_\Gamma = 2I - A_\Gamma$, where A_Γ is the adjacency matrix of Γ, and I is the identity matrix (see [21] and Section). The *Coxeter element* $\omega_\Gamma = s_1 \cdots s_k$ can be used to classify the Coxeter system. For example, if Γ is connected, then B_γ defines a *spherical*, *affine*, or *higher rank* geometry on $\mathbb{R}^\mathcal{V}$ if and only if ω_Γ is finite order, has infinite order but spectral radius 1, or has spectral radius greater than 1, respectively (see [2]). The pair $(\mathbb{R}^\mathcal{V}, B_\Gamma)$ and reflection group $\mathcal{W}_\Gamma$ with its distinguished generating reflections and Coxeter element is called the *Coxeter system* associated to Γ.

A *mixed-sign Coxeter graph* is a Coxeter graph with labels

$$\mathfrak{s} : \mathcal{V} \to \{1, -1\}.$$

The associated reflection group $\mathcal{W}_{\Gamma,\mathfrak{s}} \subset \mathrm{GL}(\mathcal{R}^{\mathcal{V}})$ is defined in an analogous way as the classical Coxeter reflection group, except that the bilinear form is replaced by $B_{\Gamma,\mathfrak{s}} = 2I_{\mathfrak{s}} - A_\Gamma$, where $I_{\mathfrak{s}}$ is the diagonal matrix with entries $\mathfrak{s}(v_i)$ on the diagonal. The relation between properties of $\omega_{\Gamma,\mathfrak{s}}$ and properties of $\mathcal{W}_{\Gamma,\mathfrak{s}}$ is more subtle than in the classical case (see [3]), and, for example, the finite order mixed-sign Coxeter reflection groups are not yet classified. However, a useful formula for the Coxeter element in terms of the adjacency matrix still holds in this setting (see Proposition 2.8).

1.3 Constructing small dilatation pseudo-Anosov mapping classes.

The first construction of infinite sequences of pseudo-Anosov mapping classes (S_n, ϕ_n), where $|\chi(S_n)|$ is unbounded and $L(S_n, \phi_n)$ is bounded, was given by Penner in [31] (see also [4] [41]). There is no evidence, however, that the conjectural minimum accumulation point for normalized dilatations γ_0^4 can be achieved by a Penner-type sequence.

Given a mapping class (S, ϕ), the *closure* of (S, ϕ) is the pair $(\overline{S}, \overline{\phi})$ where $\overline{S}$ is the closed surface obtained from S by filling in boundary components with disks, and $\overline{\phi}$ is the isotopy class of the extension to $\overline{S}$ of any homeomorphism in the equivalence class of ϕ.

Question 1.4 *For which closed oriented surfaces S can the minimum dilatation pseudo-Anosov mapping classes on S be realized as the closure of a mixed-sign Coxeter mapping class?*

The minimum dilatations are unknown for genus $g \geq 3$, however, in the orientable case, when $\lambda_{\mathrm{hom}}(\phi) = \lambda(\phi)$, the smallest dilatations, together with explicit definitions of their monodromy, were found for genus $g = 2, 3, 4, 5$ by E. Lanneau and J.-L. Thiffeault [25]. We make the following observation (see Table 2.6).

Observation 1.5 *The minimum dilatations for orientable mapping classes for genus 2,3,4, and 5 are realizable as the closures of mixed-sign Coxeter mapping classes.*

Remark 1.6 The minimum dilatation for orientable mapping classes for genus 7 was found in [1] and in [22], and for genus 8 in [17]. These examples were found using fibered face theory, and there is as yet no intrinsic description.

1.4 Lanneau-Thiffeault Question.

For orientable pseudo-Anosov mapping classes Lanneau and Thiffeault ask (see [25]) whether the minimum dilatation for orientable pseudo-Anosov mapping classes is the largest root λ_g of polynomials of the form

$$LT(x) = x^{2g} - x^{g+1} - x^g - x^{g-1} + 1,$$

for all even g. In [17] it is shown that for even g, there are orientable genus g pseudo-Anosov mapping classes (S_g, ϕ_g) with exactly two singularities whose dilatation equals λ_g. This sequence of mapping classes corresponds to a convergent sequence of points on a single fibered face, and we have

$$\lim_{g\to\infty} L(S_g, \phi_g) = \lim_{g\to\infty} (\lambda_g)^{2g} = \gamma_0^4.$$

Thus, the smallest known accumulation point for normalized dilatations, is also achieved by a sequence of orientable pseudo-Anosov mapping classes implying the following.

Theorem 1.7 *The set of normalized dilatations of closures of orientable pseudo-Anosov mixed-sign Coxeter mapping classes has accumulation point γ_0^4.*

Theorem 1.2 follows from Theorem 1.7.

To find graphs associated to small dilatation mapping classes, we use the heuristic principle that a mapping class with small dilatation should be a slight perturbation of a mapping class that is periodic. Roughly speaking, the Coxeter element of a Coxeter graph is conjugate to the homological action of its corresponding mapping class. For classical Coxeter systems, the Coxeter element is periodic if and only if the Coxeter system is spherical. These are classified, and furthermore, the spectral radius of Coxeter elements is monotone with respect to graph inclusion. Thus, for mapping classes associated to classical Coxeter systems, there is a universal lower bound on the dilatations of associated pseudo-Anosov maps (see [29] and [27]).

For mixed-sign Coxeter graphs, the spectral radius of Coxeter elements is not monotone. Thus, it is possible to find large and complicated graphs whose Coxeter elements are periodic. These are useful tools for building pseudo-Anosov mapping classes with large complexity (as measured by the Euler characteristic of the surface) and small dilatation. More precisely, we find sequences of spherical mixed-sign graphs K_n with increasing number of vertices, a fixed graph Γ_0 and concatenations $\Gamma_n = K \sharp K_n$, so that the spectral radius $\lambda(\Gamma_n)$ of the Coxeter element of Γ_n goes to 1 quickly, i.e.,

$$\log \lambda(\Gamma_n) \asymp \frac{1}{n}.$$

Murasugi sums provide a way to translate between graph theoretic perturbations, and perturbations of mapping classes. Using this idea, we prove that the sequences of mapping classes associated to K_n are the Murasugi sum of simple to understand mapping classes. We further show that mapping classes (Σ_n, ρ_n) associated to Γ_n correspond are fibrations of a single 3-manifold. Thus the Murasugi sum of (Σ_n, ρ_n) with any fixed mapping class defines a sequence (S_n, ϕ_n) whose mapping tori are homeomorphic. We call such mapping classes (S_n, ϕ_n) twisted mapping classes. Fibered face theory then implies that the sequence of normalized dilatations has accumulation points either in the interior or on the boundary of a fibered face. By arranging for the former, we obtain many sequences of mapping classes with bounded normalized dilatations.

In particular, we show that for our particular choice Γ_n, the mapping classes $(S_{\Gamma_n}, \phi_{\Gamma_n})$ correspond to points on the fibered face of the 6_2^2-link complement and converge to the minimum (S_0, ϕ_0) for normalized dilatation. By continuity of normalized dilatation on fibered faces, it then follows that

$$\lim_{n\to\infty} L(S_{\Gamma_n}, \phi_{\Gamma_n}) = \gamma_0^4.$$

1.5 Organization.

We begin in Section 2 with definitions of mixed-sign Coxeter systems $\Gamma, \mathfrak{s}$ and their properties, particularly in relation to the Artin group $\mathcal{A}_\Gamma$ associated to Γ. We also define a surface S_Γ associated to Γ given an ordering on the vertices and a fat graph structure. Then the Artin group $\mathcal{A}_\Gamma$ acts as mapping classes on S_Γ, and for each choice of signs $\mathfrak{s}$ on Γ, we define a particular element $\phi_{\Gamma,\mathfrak{s}}$ depending on an ordering on Γ. If Γ is bipartite, then this is the same as examples studied by Thurston [38] and Leininger [27]. In Section 3, we define twisted mapping classes and prove Theorem 1.7.

Acknowledgments: I am grateful to the Tokyo Institute of Technology and University of Tokyo for their support during the writing of this paper, and J. F. Valdez and J. Mangahas for helpful conversations.

2 Mixed-sign Coxeter systems and associated mapping classes.

In this section we define a correspondence between various objects associated to a mixed-sign Coxeter graph. The following table summarizes the main objects.

Data	**Object**	**Notation**
mixed sign graph $\Gamma, \mathfrak{s}$	Mixed-sign Coxeter system	$(\mathcal{W}_{\Gamma,\mathfrak{s}}, \mathcal{R}_{\Gamma,\mathfrak{s}})$
ordered mixed sign graph $\Gamma, \mathfrak{s}$	Mixed-sign Coxeter element	$\omega_{\Gamma,\mathfrak{s}}$
graph Γ	Artin group and representation	$\rho_\Gamma : \mathcal{A}_\Gamma \to GL(\mathbb{R}^{\mathcal{V}})$
ordered fatgraph Γ	geometric realization	$(S_\Gamma, \mathcal{C}_\Gamma)$
ordered mixed sign fatgraph $\Gamma, \mathfrak{s}$	Coxeter mapping class	$(S_\Gamma, \phi_{\Gamma,\mathfrak{s}})$

Given an ordered mixed-sign Coxeter graph, $(\Gamma, \mathfrak{s})$ we define a reflection group $\mathcal{W}_{\Gamma,\mathfrak{s}}$ in Section 2.1, and a representation of the Artin group $\mathcal{A}_\Gamma$

$$\rho_\Gamma : \mathcal{A}_\Gamma \to GL(\mathbb{R}^{\mathcal{V}})$$

in Section 2.2. When Γ has a fatgraph structure, we define an associated geometric realization $(S_\Gamma, \mathcal{C}_\Gamma)$ of Γ, and a mapping class $\phi_{\Gamma,\mathfrak{s}} : S_\Gamma \to S_\Gamma$ (Section 2.3). The groups $\mathcal{A}_\Gamma$ and $\mathcal{W}_{\Gamma,\mathfrak{s}}$ come with k standard generators $\{\sigma_1, \dots, \sigma_k\}$ and $\{s_1, \dots, s_k\}$, respectively. Let σ and w be the epimorphisms of the free group $\langle x_1, \dots, x_k \rangle$ to $\mathcal{A}_\Gamma$ and $\mathcal{W}_{\Gamma,\mathfrak{s}}$, where $\sigma(x_i) = \sigma_i$ and $w(x_i) = s_i$.

$$\begin{array}{ccccccc} \langle x_1, \dots, x_k \rangle & \xrightarrow{\sigma} & \mathcal{A}_\Gamma & \xrightarrow{\rho_\Gamma} & GL(\mathbb{R}^{\mathcal{V}}) & \xrightarrow{\eta} & GL(H_1(S_\Gamma; \mathbb{R})) \\ & \searrow^{w} & & & & & \\ & & \mathcal{W}_{\Gamma,\mathfrak{s}} & \xrightarrow{\subset} & GL(\mathbb{R}^{\mathcal{V}}). & & \end{array}$$

Let $\omega_{\Gamma,\mathfrak{s}} = w(x_1 \cdots x_k)$, called the *(mixed-sign) Coxeter element*. Write $\mathfrak{s}(i) = \mathfrak{s}(v_i)$, and let $\sigma_{\Gamma,\mathfrak{s}} = \rho_\Gamma(\sigma_1^{\mathfrak{s}(1)} \cdots \sigma_k^{\mathfrak{s}(k)})$. The representations ρ_Γ and η preserve symplectic forms, while the elements of

$\mathcal{W}_{\Gamma,\mathfrak{s}}$ preserve a symmetric one, but we will show

$$\omega_{\Gamma,\mathfrak{s}} = -\sigma_{\Gamma,\mathfrak{s}}$$

as elements of $GL(\mathbb{R}^{\mathcal{V}})$ (Proposition 2.6). The element $\sigma_{\Gamma,\mathfrak{s}}$ satisfies

$$\eta(\rho_\Gamma(\sigma_{\Gamma,\mathfrak{s}})) = (\phi_{\Gamma,\mathfrak{s}})_*$$

and hence the homological dilatation of $\phi_{\Gamma,\mathfrak{s}}$ and the spectral radius of the Coxeter element $\omega_{\Gamma,\mathfrak{s}}$ satisfy

$$\lambda_{\text{hom}}(\phi_{\Gamma,\mathfrak{s}}) = |\omega_{\Gamma,\mathfrak{s}}|$$

(see Proposition 2.12). From this we derive a sufficient condition for a mixed-sign Coxeter mapping class to be pseudo-Anosov (see Proposition 2.13).

Mixed-sign Coxeter mapping classes are defined on surfaces with boundary, but in some cases the dynamical information contained in the mapping class extends to the closure of the surface obtained by filling in disks. This is discussed in Section 2.4. The special case of mapping classes associated to bipartite Coxeter graphs is treated in Section 2.5. Section 2.6 gives a table of mixed-sign Coxeter graphs associated to minimum dilatation orientable pseudo-Anosov mapping classes for small genus.

Remark 2.1 The study of mapping classes using Coxeter graphs and associated reflection groups has a long history in algebraic geometry dating back to the 19th century, particularly in the study of complex surface singularities (see [34], [10] and references therein). The focus in geometric topology has on the other hand been on representations of the Artin group of a Coxeter graph into the mapping class group (see, for example, [24]). The difference comes from the fact the associated bilinear forms left invariant by the respective automorphism groups are different: one being symmetric and the other symplectic. From this point of view our results concerning special elements of the Artin group, and Coxeter elements of the Coxeter reflection group are part of an overlap in the two theories (see also [40] [19]).

2.1 Mixed-sign Coxeter reflection group

In this section we define mixed-sign Coxeter systems as a slight generalization of classical simply-laced Coxeter systems. Let $(\Gamma, \mathfrak{s})$ be a mixed-sign Coxeter graph with ordered vertices $\mathcal{V} = \{v_1, \ldots, v_n\}$ and map $\mathfrak{s} : \mathcal{V} \to \{\pm 1\}$. For $i, j = 1, \ldots, k$, define

$$m_{i,j} = \begin{cases} 1 & \text{if } i = j \\ 2 & \text{if } v_i \text{ and } v_j \text{ are not connected by an edge} \\ 3 & \text{if } v_i \text{ and } v_j \text{ are connected by an edge.} \end{cases}$$

Remark 2.2 In the usual definition of Coxeter and Artin groups, the $m_{i,j}$ are allowed to vary (for $i \neq j$) in the set $\{2, 3, \ldots, \infty\}$. In this paper, we restrict only to the *simply-laced case* described above.

Let $I_{\mathfrak{s}}$ be the $n \times n$ matrix with 0 on the off-diagonal, and diagonal entries equal to $\mathfrak{s}(1), \ldots, \mathfrak{s}(n)$. Let $A = [a_{i,j}]$ be the adjacency matrix of Γ, A^+ the upper triangular part of A, and $U = I_{\mathfrak{s}} - A^+$. Then U determines a symmetric form

$$B = U + U^T$$

on V.

The Coxeter system $(\mathcal{W}, \mathcal{R}) = (\mathcal{W}_{\Gamma,\mathfrak{s}}, \mathcal{R}_{\Gamma,\mathfrak{s}})$ associated to $(\Gamma, \mathfrak{s})$ is the subgroup of $\mathrm{GL}(\mathbb{R}^{\mathcal{V}})$ generated by $\mathcal{R}_{\Gamma,\mathfrak{s}} = \{s_1, \ldots, s_n\}$, where the s_i are defined by

$$\begin{aligned} s_i(v_j) &= v_j - 2\frac{B(v_i, v_j)}{B(v_I, v_I)} v_i \\ &= \begin{cases} -v_j & \text{if } i = j, \\ v_j + \mathfrak{s}(i) a_{i,j} v_i & \text{if } i \neq j. \end{cases} \end{aligned}$$

Each s_i can be interpreted as a reflection through the hyperplane perpendicular to v_i in $\mathbb{R}^{\mathcal{V}}$ with respect to the symmetric form B. If $\mathfrak{s} \equiv 1$, then $(\mathcal{W}, \mathcal{R})$ is the classical Coxeter system.

Given a mixed-sign ordered Coxeter graph $(\Gamma, \mathfrak{s})$, we define the *Coxeter element* to be

$$\omega_{\Gamma,\mathfrak{s}} = s_1 \cdots s_n \in \mathcal{W}_{\Gamma,\mathfrak{s}}.$$

Coxeter systems $(\mathcal{W}, \mathcal{R})$, and more generally reflection systems, are classified by the type of associated bilinear form B. If B is positive or negative definite, we say $(\mathcal{W}, \mathcal{R})$ is *spherical*, if B is positive or negative semi-definite, then we say $(\mathcal{W}, \mathcal{R})$ is *affine*, and if the signature of B is (p, q), where p and q are nonzero we say $(\mathcal{W}, \mathcal{R})$ is *higher rank*. (see [21]). For classical Coxeter systems, these are the only cases that occur.

The classical (simply-laced) Coxeter systems $(\mathcal{W}, \mathcal{R})$ and their Coxeter elements ω_Γ, where $\mathfrak{s} \equiv 1$, have the following special properties (see, for example, [6] [2] [29]).

(i) (*Presentation.*) The Coxeter group $\mathcal{W}$ has presentation in terms of the standard generators $\mathcal{R} = \{s_1, \ldots, s_k\}$:

$$\langle s_1, \ldots, s_k \ : \ (s_i s_j)^{m_{i,j}} \rangle.$$

(ii) (*Monotonicity.*) The spectral radius of Coxeter elements is monotone increasing with respect to inclusion of Coxeter graphs that respect orderings on vertices. If Γ_1 and Γ_2 are both higher rank and $\Gamma_1 \subsetneq \Gamma_2$, then the spectral radius of Γ_2 is strictly higher than that of Γ_1.

(iii) (*Bipartite Coxeter eigenvalue.*) The spectral radius of Coxeter elements is bounded from below by

$$\frac{(\mu^2 - 2) + \sqrt{(\mu^2 - 2)^2 - 4}}{2},$$

known as the *bipartite eigenvalue* of the Coxeter system.

These properties do not necessarily hold for mixed-sign Coxeter systems (see [3]).

Example 2.3 If v_i and v_j are two adjacent vertices on Γ, and $\mathfrak{s}(i) \neq \mathfrak{s}(j)$, then $s_i s_j$ has infinite order.

Example 2.4 The mixed-sign Coxeter graph $(\Gamma, \mathfrak{s})$, where Γ is the complete graph on 3 vertices, and $\mathfrak{s} \equiv -1$, is spherical. The Coxeter group is isomorphic to the symmetric group on 4 letters, while the three generator group with only the pairwise relations is isomorphic to the affine group associated to $\widetilde{A_2} = (\Gamma, +1)$ and has infinite order.

Example 2.5 Property (ii), the monotonicity property, of classical Coxeter elements implies that there is a lower bound greater than 1 for the spectral radius of classical Coxeter elements of non-spherical or affine Coxeter graphs. For classical Coxeter elements with $\mu^2 > 2$, the smallest positive spectral radius is Lehmer's number

$$\lambda_L \approx 1.17628$$

(see [29]), which is also the smallest possible bipartite eigenvalue of a non-spherical and non-affine Coxeter graph. On the other hand, as we see later in this paper, the spectral radius of mixed-sign Coxeter elements can be made arbitrarily close to one.

2.2 Representations of Artin groups

We recall the definition of the Artin group $\mathcal{A}_\Gamma$ associated to a Coxeter graph Γ, and define representations of $\mathcal{A}_\Gamma$ associated to an ordered mixed-sign Coxeter graph $(\Gamma, \mathfrak{s})$ (see, for example, [5] and references therein).

The *Artin group* of Γ is the group

$$\mathcal{A}_\Gamma = \langle \sigma_1, \ldots, \sigma_n \ : \ [\sigma_i \sigma_j]_{m_{i,j}} = [\sigma_j \sigma_i]_{m_{i,j}} \rangle$$

where $[\sigma_i \sigma_j]_m$ is the alternating product

$$[\sigma_i \sigma_j]_m = \sigma_i \sigma_j \sigma_i \ldots$$

of length m. If Γ is the classical Coxeter graph A_n, then $\mathcal{A}_\Gamma$ is the braid group on the disk with $n+1$ punctures.

Let $\mathbb{R}^{\mathcal{V}}$ be the vector space of real labels on the vertices of Γ. The ordered vertices $\mathcal{V}$ determine an ordered basis $v_1, \ldots, v_n$ of $\mathbb{R}^{\mathcal{V}}$. Let A be the adjacency matrix for Γ. Let F be the skew-symmetric bilinear form on $\mathbb{R}^{\mathcal{V}}$ defined with respect to $v_1, \ldots, v_n$ by

$$F = A^+ - A^-,$$

where A^+ is the upper triangular part of A, and A^- is the lower triangular part. The matrix F defines a skew symmetric form on $\mathbb{R}^{\mathcal{V}}$ that depends on the choice of ordering of $\mathcal{V}$.

Let $\mathfrak{s}$ be a sign-labeling for Γ. Define ρ_Γ to be the representation

$$\rho_\Gamma : \mathcal{A}_\Gamma \to \mathrm{GL}(\mathbb{R}^{\mathcal{V}})$$

preserving F defined by

$$\begin{aligned}\rho_\Gamma(\sigma_i)(v_j) &= v_j + F(v_i, v_j)v_i \\ &= \begin{cases} v_j & \text{if } i = j, \\ v_j + a_{i,j}v_i & \text{if } i < j, \\ v_j - a_{i,j}v_i & \text{if } i > j. \end{cases}\end{aligned}$$

Then the image preserves F. We call ρ_Γ the *Artin representation* of $\mathcal{A}_\Gamma$. Define

$$\sigma_{\Gamma,\mathfrak{s}} = \sigma_1^{\mathfrak{s}(1)} \cdots \sigma_k^{\mathfrak{s}(k)}$$

to be the *Artin element* associated to the ordered mixed-sign Coxeter graph.

Proposition 2.6 *The Coxeter element $\omega_{\Gamma,\mathfrak{s}}$ and the Artin element $\sigma_{\Gamma,\mathfrak{s}}$ are related by*

$$\omega_{\Gamma,\mathfrak{s}} = -\rho_\Gamma(\sigma_{\Gamma,\mathfrak{s}}).$$

Let $B_c = U + cU^T$, for $c \in \mathbb{C} \setminus 0$. Then we have $B = B_1$ and $F = B_{-1}$. Now define elements $f_1^{(c)}, \ldots, f_n^{(c)} \in \mathrm{GL}(\mathbb{R}^{\mathcal{V}})$ by

$$\begin{aligned}f_i^{(c)}(v_j) &= v_j - \mathfrak{s}(i)B_c(i,j)v_i \\ &= \begin{cases} -cv_i & \text{if } i = j \\ v_j + \mathfrak{s}(i)a_{i,j}v_i & \text{if } i < j \\ v_j + c\mathfrak{s}(i)a_{i,j}v_i & \text{if } i > j \end{cases}\end{aligned}$$

Then $f_i^{(1)} = s_i$ and $f_i^{(-1)} = \rho_\Gamma(\sigma_i^{\mathfrak{s}(i)})$.

Proposition 2.6 follows from the following generalization of a result of Howlett [20].

Lemma 2.7 *Using the above notation*

$$f_1^c \cdots f_n^c = -cU^{-1}U^T.$$

We present the generalized proof here.

Proof of Lemma 2.7. First we notice that

$$\begin{aligned}Uf_1^{(c)} &= \begin{bmatrix} \mathfrak{s}(1) & -a_{1,2} & -a_{1,3} & \ldots & -a_{1,n} \\ 0 & \mathfrak{s}(1) & -a_{2,3} & \ldots & -a_{2,n} \\ \ldots & & & & \\ 0 & & & \ldots & \mathfrak{s}(n) \end{bmatrix} \begin{bmatrix} -c & \mathfrak{s}(1)a_{1,2} & & \ldots & \mathfrak{s}(1)a_{1,n} \\ 0 & 1 & 0 & \ldots & 0 \\ \ldots & & & & \\ 0 & & & & 1 \end{bmatrix} \\ &= \begin{bmatrix} -c\mathfrak{s}(1) & 0 & & \ldots & 0 \\ 0 & \mathfrak{s}(1) & -a_{2,3} & \ldots & -a_{2,n} \\ \ldots & & & & \\ 0 & & & \ldots & \mathfrak{s}(n) \end{bmatrix}\end{aligned}$$

Assume that

$$
\begin{aligned}
U f_1^{(c)} \cdots f_k^{(c)} &= \begin{bmatrix}
-c\mathfrak{s}(1) & 0 & & & \cdots & & & 0 \\
-ca_{1,2} & -c\mathfrak{s}(1) & 0 & & & & \cdots & 0 \\
 & \cdots & & & & & & \\
-ca_{k,1} & \cdots & -ca_{k,k-1} & -c\mathfrak{s}(k) & 0 & & \cdots & 0 \\
0 & & \cdots & 0 & \mathfrak{s}(k+1) & -a_{k+1,k+2} & \cdots & -a_{k+1,n} \\
 & \cdots & & & & & & \\
0 & & & \cdots & & 0 & \mathfrak{s}(n-1) & -a_{n-1,n} \\
0 & & & \cdots & & & 0 & \mathfrak{s}(n)
\end{bmatrix} \\
&= \begin{bmatrix} L_k & 0 \\ 0 & U_k \end{bmatrix}.
\end{aligned}
$$

Multiplying on the right by

$$
f_{k+1}^{(c)} = \left[\begin{array}{c|c|c}
I & 0 & 0 \\ \hline
-\mathfrak{s}(k+1)ca_{k+1,1} \cdots -\mathfrak{s}(k+1)ca_{k+1,k} & -c & \mathfrak{s}(k+1)a_{k+1,k+2} \ldots \mathfrak{s}(k+1)a_{k+1,n} \\ \hline
0 & 0 & I
\end{array}\right]
$$

amounts to replacing the $k+1$st row of $U f_1^{(c)} \cdots f_k^{(c)}$ by

$$[a_{k+1,1}, \ldots, a_{k+1,k}, -\mathfrak{s}(k+1), 0, \ldots, 0].$$

Thus,

$$U f_1^{(c)} \cdots f_{k+1}^{(c)} = \begin{bmatrix} L_{k+1} & 0 \\ 0 & U_{k+1} \end{bmatrix}$$

and $L_n = -cU^T$ as desired. □

For each c, the transformation $f = f_1^{(c)} \cdots f_n^{(c)}$ satisfies

$$f^T B_c f = B_c.$$

The following consequence of Lemma 2.7 completes the proof of Proposition 2.6.

Proposition 2.8 *The mixed-sign Coxeter element and representation of the corresponding element of the Artin group is given by*

$$\omega_{\Gamma,\mathfrak{s}} = -U^{-1}U^T,$$

and

$$\rho_\Gamma(\sigma_{\Gamma,\mathfrak{s}}) = U^{-1}U^T.$$

2.3 Geometric realization and mixed-sign Coxeter mapping class

In this section, we define a compact oriented surface S_Γ from an ordered Coxeter fatgraph Γ, and a mapping class $\phi_{\Gamma,\mathfrak{s}}$ from Γ and a sign-labeling s.

Let Γ be a Coxeter graph with vertices $\mathcal{V}$. A *fatgraph* (or *ribbon*) structure on Γ is a choice of cyclic ordering on the edges emanating from each vertex of $\mathcal{V}$. For any embedding of a graph Γ on a surface S there is a corresponding fat graph structure on Γ. Conversely, for any fat graph structure on Γ there is a unique oriented closed surface on which Γ embeds as a fat graph so that the complementary components are disks.

Let

$$\mathfrak{o} : \mathcal{V} \to \{1, \ldots, n\}$$

be the bijection corresponding to the ordering on $\mathcal{V}$. For each $v \in \mathcal{V}$, let $\mathcal{V}_v \subset \mathcal{V}$ be the link of v, i.e., the set of vertices connected to v by an edge. Then the fat graph structure of Γ is equivalent to a choice of cycle

$$\sigma_v = (i_1, \ldots, i_k),$$

in the symmetric group $\mathcal{S}_n$ on n elements for each element $v \in \mathcal{V}$ with $\mathcal{V}_v = \{v_{i_1}, \ldots, v_{i_k}\}$.

Construct a system of annuli T_v, for $v \in \mathcal{V}$, with oriented core curve γ_v so that

1. T_v and T_w are glued together along a square patch if and only if v and w are connected by an edge;
2. if $\mathfrak{o}(v) < \mathfrak{o}(w)$, then $i_{\text{alg}}(\gamma_v, \gamma_w) > 0$; and
3. If v is a vertex, then for each of the the core curves γ_w, for $w \in \mathcal{V}_v$, intersect γ_v in a cyclic ordering that respects the orientation of ℓ_v and cycle σ_v.

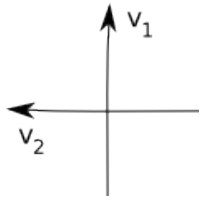

Figure 1: Positive intersection

Here we use the convention that if γ_i and γ_j intersect as in Figure 1, then $i_{\text{alg}}(\gamma_i, \gamma_j) = 1$.

Figure 2 shows the arrangement of $T_{v_1}, T_{v_2}, T_{v_3}$ and T_v where $\sigma_v = (1, 2, 3)$, and $\mathfrak{o}(v_2) < \mathfrak{o}(v) < \mathfrak{o}(v_1), \mathfrak{o}(v_3)$.

The arrows in the figure indicate which vertex comes before the other in the global ordering. One sees that the surface depends on the relative global ordering of adjacent vertices and the fatgraph structure.

Let $\mathfrak{s}$ be a sign-labeling for Γ. Let $\phi_{\Gamma,\mathfrak{s}} S_\Gamma \to S_\Gamma$ be the mapping class defined by

$$\phi_{\Gamma,\mathfrak{s}} = (\delta_1)^{\mathfrak{s}(1)} \cdots (\delta_k)^{\mathfrak{s}(k)},$$

where δ_i are the right Dehn twists centered at γ_i. (See, for example, [12] for definition of Dehn twist.) Then $(S_\Gamma, \phi_{\Gamma,\mathfrak{s}})$ is the *Coxeter mapping class* associated to $(\Gamma, \mathfrak{s})$.

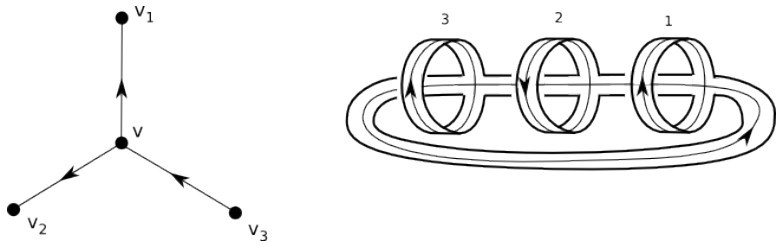

Figure 2: A local picture of Coxeter graph and corresponding union of annuli

Figure 3 gives an illustration of the action of a right Dehn twist on a transversally intersecting curve. One may verify that $\delta_i(\gamma_j) = \gamma_j + \gamma_i$ when γ_i and γ_j are oriented in this way with $i_{\text{alg}}(\gamma_i, \gamma_j) = 1$.

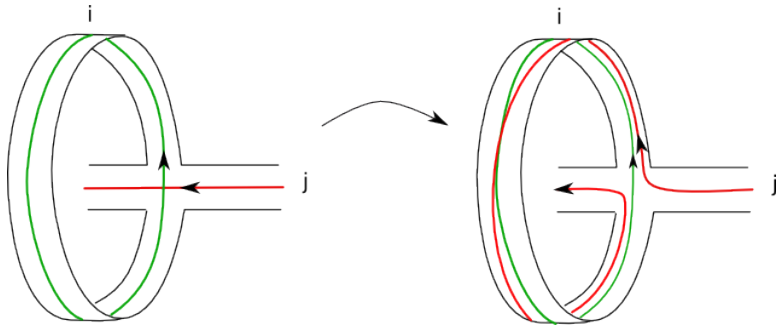

Figure 3: Right Dehn twist along δ_i acting on γ_j, where $i < j$.

Remark 2.9 The surfaces S_Γ depend only on the choice of vertex ordering and fatgraph structure on Γ. Different vertex orderings and fatgraph structures can give rise to different homeomorphism types of surfaces.

By contrast, the topological Euler characteristic of S_Γ is independent of the ordering and fatgraph structure.

Lemma 2.10 *Let S_Γ be a geometric realization of Γ. Then $\chi(S_\Gamma) = -|\mathcal{E}|$, where $|\mathcal{E}|$ is the total number of edges of Γ. In particular, $\chi(S_\Gamma)$ does not depend on the ordering of $\mathcal{V}$ or the fatgraph structure.*

Proof. The construction of S_Γ is inductive with respect to an ordering on the vertices $\mathcal{V} = \{v_1, \ldots, v_k\}$. At each stage i we attach an annulus to the preceding surface along patches one for each vertex v_j adjacent to v_i such that $j < i$. The Euler characteristic thus changes by the number of such vertices. Thus each edge is counted exactly once. □

Remark 2.11 We could extend the definition of $(S_\Gamma, \phi_{\Gamma,\mathfrak{s}})$ further, by replacing $\mathfrak{s}$ with

$$\epsilon : \mathcal{V} \to \mathbb{Z}^*,$$

where $\mathbb{Z}^*$ is the set of nonzero integers, and setting

$$\phi_{\Gamma,\epsilon} = \delta_1^{\epsilon_1} \circ \cdots \circ \delta_n^{\epsilon_n}.$$

Each $\phi_{\Gamma,\epsilon}$ is, however, also associated to a signed graph. The signed graph $(\Gamma', \mathfrak{s})$ is obtained from (Γ, ϵ) by successively replacing each vertex v_i in Γ with $m_i = |\epsilon_n|$ copies $v_i^{(j)}$. Each of the new vertices $v_i^{(j)}$ of Γ' has edges connecting it to all the vertices to which v_i was connected. The new sign labels on $v_i^{(j)}$ equal the sign of ϵ.

Let $\mathbb{R}^{\mathcal{V}} \hookrightarrow H_1(S_\Gamma; \mathbb{R})$ be the linear map defined by sending the ith basis vector to $[\gamma_i]$. Let $GL(\mathbb{R}^{\mathcal{V}}) \to GL(H_1(S_\Gamma; \mathbb{R}))$ be the homomorphism defined by extending by the identity on the complementary space of the image of $\mathbb{R}^{\mathcal{V}}$.

Proposition 2.12 *The induced map $(\phi_{\Gamma,\mathfrak{s}})_* : H_1(S_\Gamma; \mathbb{R}) \to H_1(S_\Gamma; \mathbb{R})$ on homology satisfies*

$$(\phi_{\Gamma,\mathfrak{s}})_* = \rho_\Gamma(\sigma_{\Gamma,\mathfrak{s}})$$

and hence

$$\lambda_{hom}(\phi_{\Gamma,\mathfrak{s}}) = |\omega_{\Gamma,\mathfrak{s}}|.$$

Proof. Let $g_i = [\gamma_i]$ be the homology classes. The choice of orientations and algebraic intersections of $g_1, \ldots, g_k$ satisfy

$$(\delta_i)_*(g_j^{\mathfrak{s}(i)}) = \begin{cases} g_j & \text{if } i = j \\ g_j + \mathfrak{s}(i) g_i & \text{if } i < j \\ g_j - \mathfrak{s}(i) g_i & \text{if } i > j. \end{cases}$$

This can be checked by examining Figure 3. Thus, $(\delta_i)_*^{\mathfrak{s}(i)}$ restricted to the image of $\mathbb{R}^{\mathcal{V}}$ in $H_1(S_\Gamma; \mathbb{R})$ equals $\rho_\Gamma(\sigma_i)$. □

Proposition 2.13 *If Γ is connected and the spectral radius of the Coxeter element $|\omega_{\Gamma,\mathfrak{s}}|$ is greater than one, then $(S_{\Gamma,\mathfrak{s}}, \phi_{\Gamma,\mathfrak{s}})$ is pseudo-Anosov, and the dilatation satisfies*

$$\lambda(\phi_{\Gamma,\mathfrak{s}}) \geq |\omega_{\Gamma,\mathfrak{s}}|.$$

Proof. By the Nielsen-Thurston classification, any mapping class is either periodic, reducible or pseudo-Anosov [38]. Since Γ is connected, ω_Γ is irreducible, and hence so is the homological action of ϕ_Γ. This implies that ϕ_Γ is not reducible.

Since $\lambda_{\text{hom}}(\phi_{\Gamma,\mathfrak{s}}) > 1$, $\phi_{\Gamma,\mathfrak{s}}$ is not periodic, so it must be pseudo-Anosov. The rest follows from the following well-known inequality (see, e.g. [33]).

$$\lambda_{\text{hom}}(\phi) \leq \lambda_{\text{geo}}(\phi).$$

□

2.4 Mapping classes on closures and interiors

Let S be a compact surface, we have defined the mapping class group $\mathrm{Mod}(S)$ to be the group of isotopy classes of orientation preserving self-homeomorphisms of S up to isotopy relative to the boundary of S. Consider the interior $\mathrm{int}(S)$ of S. Topologically, this is homeomorphic to a surface with punctures one for each boundary component of S. Let $\mathrm{Mod}(\mathrm{int}(S))$ be the group of orientation preserving self-homeomorphisms on $\mathrm{int}(S)$ modulo isotopy. Then the map

$$\alpha : \mathrm{Mod}(S) \to \mathrm{Mod}(\mathrm{int}(S)) \tag{2}$$

defined by restriction has kernel generated by Dehn twists centered at boundary parallel simple closed curves.

The following results are well-known, and are contained for example in [5].

Lemma 2.14 *If (S, ϕ) is a pseudo-Anosov element of Mod(S), then $\alpha(S, \phi)$ is also pseudo-Anosov, and the dilatations are the same.*

Proof. If (S, ϕ) is pseudo-Anosov, and $(\mathcal{F}^{\pm}, \nu^{\pm})$ are its associated stable and unstable foliations, then $(\mathcal{F}^{\pm}, \nu^{\pm})$ also define stable and unstable foliations for $\alpha(S, \phi)$, and the stretching factor λ is also preserved. □

Let $\overline{S}$ be the closed surface obtained by filling in the boundary components of S with disks. Then there is a homomorphism

$$\beta : \mathrm{Mod}(S) \to \mathrm{Mod}(\overline{S}) \tag{3}$$

defined by extending over disks. This map is neither one-to-one nor onto. Furthermore, the image of a pseudo-Anosov mapping class is not necessary pseudo-Anosov. We will write $(\overline{S}, \overline{\phi}) = \beta(S, \phi)$.

Lemma 2.15 *If (S, ϕ) is pseudo-Anosov, and none of the boundary components are 1-pronged, then $(\overline{S}, \overline{\phi})$ is also pseudo-Anosov with dilatation $\lambda(\overline{\phi}) = \lambda(\phi)$.*

The idea of the proof is that if there are no 1-pronged boundary components, then the stable and unstable foliations of (S, ϕ) determine invariant transverse measured foliations for $\overline{\phi}$ with expansion factor $\lambda^{\pm 1}$ for $\lambda = \lambda(\phi)$ (see, for example, [18], Lemma 2.5).

We can also refine Lemma 2.15 as follows. Let (S, ϕ) be a mapping class, where S is compact. For any boundary component b of S, let $b = b_1, \ldots, b_s$ be the orbit of b under the action of ϕ. Let $cl(S, b)$ be the surface obtained by filling in the boundary components $b_1, \ldots, b_s$ with disks, and let $cl(\phi, b)$ be the extension of ϕ. Let $cl(S, \phi, b) = (cl(S, b), cl(\phi, b))$. If (S, ϕ) is pseudo-Anosov, and b is m-pronged, then all orbits of b are also m-pronged.

Lemma 2.16 *If (S, ϕ) is pseudo-Anosov, then $(cl(S, b), cl(\phi, b))$ is pseudo-Anosov if the boundary components $b_1, \ldots, b_s$ are not 1-pronged. In this case,*

$$\lambda(cl(\phi)) = \lambda(\phi).$$

The proof is the same as for Lemma 2.15.

2.5 Bipartite graphs

In this section we collect some special properties of mixed-sign Coxeter systems, and mixed-sign Coxeter mapping classes associated to bipartite graphs.

A Coxeter graph Γ is *bipartite (with bipartite ordering)* if the following hold:

(i) its vertices can be separated into two disjoint sets $\mathcal{V} = \mathcal{V}_1 \cup \mathcal{V}_2$ where the subgraph of Γ generated by $\mathcal{V}_i$ has no edges for $i = 1, 2$; and

(ii) by the ordering on $\mathcal{V}$ has the property that the elements of $\mathcal{V}_1$ proceed all the elements of $\mathcal{V}_2$.

A graph Γ is bipartite if and only if it contains no odd cycles. Given a sign-labeling $\mathfrak{s}$ of a Coxeter graph Γ. Let $\overline{\mathfrak{s}}$ be the sign-labeling defined by $\overline{\mathfrak{s}}(v) = -\mathfrak{s}(v)$ for all $v \in \mathcal{V}$.

Theorem 2.17 *If Γ is bipartite, and $\mathfrak{s}$ is any sign-labeling on Γ, then $(\mathcal{W}_{\Gamma,\mathfrak{s}}, \mathcal{R}_{\Gamma,\mathfrak{s}})$ and $(\mathcal{W}_{\Gamma,\overline{\mathfrak{s}}}, \mathcal{R}_{\Gamma,\overline{\mathfrak{s}}})$ are conjugate as subgroups of $GL(\mathcal{R}^{\mathcal{V}})$, and, in particular, the spectral radius of Coxeter elements satisfies*

$$|\omega_{\Gamma,\mathfrak{s}}| = |\omega_{\Gamma,\overline{\mathfrak{s}}}|.$$

Proof. It suffices to show that the generating sets $\mathcal{R}_{\Gamma,\mathfrak{s}} = \{s_1, \ldots, s_k\}$ and $\mathcal{R}_{\Gamma,\overline{\mathfrak{s}}} = \{\overline{s}_1, \ldots, \overline{s}_k\}$ are conjugate as elements of $GL(\mathbb{R}^{\mathcal{V}})$.

let $\mathcal{V} = \mathcal{V}_1 \cup \mathcal{V}_2$ be the bipartite partition. Let k_i be the number elements in $\mathcal{V}_i$, for $i = 1, 2$, and let $k = k_1 + k_2$ be the total number of vertices $\mathcal{V}$. Let I_{k_1,k_2} be the $k \times k$ diagonal matrix with the first k_1 diagonal entries equal to 1 and the second k_2 diagonal entries equal to -1. Then s_i and s_i' satisfy

$$s_i = I_{k_1,k_2} \overline{s}_i I_{k_1,k_2}.$$

□

If a graph Γ is bipartite, and is given the bipartite ordering, then there is a fatgraph structure on Γ so that after cutting each annulus at a transversal arc between the two boundary components, the surface can be placed on a plane as a union of rectangles oriented in vertical and horizontal directions as in Figure 4. The right diagram in Figure 4 gives the corresponding surface S_Γ.

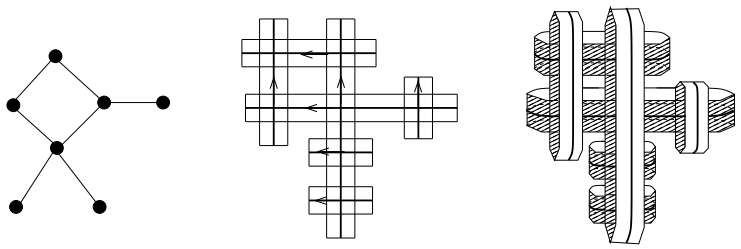

Figure 4: Surface associated to a bipartite graph

The *bipartite eigenvalue* of a graph Γ is defined by

$$\beta_\Gamma = |x^2 - (2 - \mu^2)x + 1|,$$

where μ is the spectral radius of the adjacency matrix of Γ. Note, this does not depend on the ordering of the vertices of Γ.

The following theorem was proved for (positively signed) classical Coxeter graphs Γ in [29].

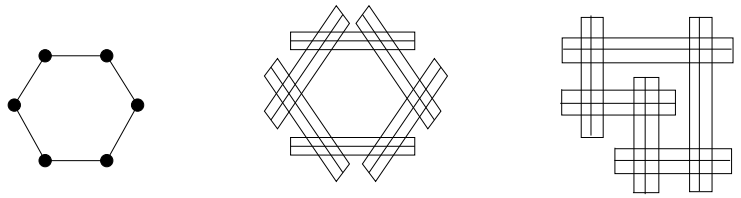

Figure 5: Two surfaces obtained from the hexagonal graph by identifying opposite short edges of the rectangles.

Theorem 2.18 *Let Γ be a positively signed bipartite Coxeter graph with bipartite ordering. Let μ be the spectral radius of the adjacency matrix of Γ. Then either $|\mu^2 - 2| \leq 2$, which implies that $|\omega_{\Gamma,1}| = 1$, or*

$$|\omega_{\Gamma,1}| = \beta_\Gamma$$

and hence only depends on the combinatorics of Γ. Furthermore, for any arbitrary (positively signed) Coxeter graph Γ, with arbitrary ordering on the vertices,

$$|\omega_{\Gamma,1}| \geq \beta_\Gamma.$$

In [38], Thurston gave an example of pseudo-Anosov mapping classes constructed using classical bipartite Coxeter graphs. These are mixed-sign Coxeter mapping classes associated to a bipartite Coxeter graph, with bipartite order. He proved the following.

Theorem 2.19 *If Γ is a classical bipartite Coxeter graph with bipartite order, then the widths and lengths of the rectangles in the construction of S_Γ can be chosen so that $\phi_{\Gamma,\mathfrak{s}}$ has constant derivative. If ϕ_Γ is pseudo-Anosov, then*

$$\lambda_{geo}(\phi_{\Gamma,\mathfrak{s}}) = \lambda_{hom}(\phi_{\Gamma,\mathfrak{s}}) = \beta_\Gamma.$$

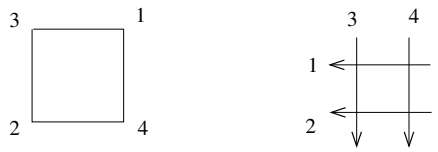

Figure 6: Dual configuration associated to a 4 cycle with bipartite ordering

Example 2.20 Consider the hexagonal graph shown Γ_6 in Figure 5. Since each vertex has order two, there is only one fatgraph structure on Γ_6. For the middle diagram, there is no way to orient the core curves on the rectangles in a way that is orientation compatible with any ordering on Γ_6. The orientation on one curve determines the orientations on its adjacent ones. Thus, a $2n$-gon has an orientation compatible diagram of this form if and only if n is even. The right diagram is compatible with the bipartite ordering. In this example, the middle surface has genus 2 and 4 boundary components, while the right hand surface has genus 3 and 2 boundary components.

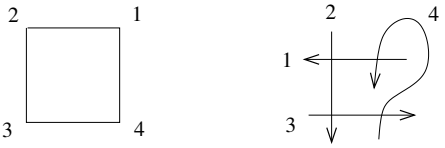

Figure 7: Dual configuration associated to a 4 cycle with cyclic ordering

Example 2.21 It also may not be possible to make the surface from a globally planar configuration of straight paths, as one can in the bipartite case. Consider for example the cyclic graph with 4 vertices. The bipartite ordering gives rise to a planar configuration (see Figure 6), while for the cyclic ordering, one can verify that there is no configuration of straight line paths that realize the graph (see Figure 7). This example also illustrates that while the graph determines the Euler characteristic of the surface (with boundary), but ordering of the vertices can affect the genus. In the bipartite case, the surface has $(g, n) = (1, 4)$, while in the cyclic case the surface has $(g, n) = (2, 2)$.

2.6 Minimum dilatation orientable examples.

Table 1 displays mixed-sign Coxeter graphs that give rise to the minimum dilatation orientable mapping classes of genus 2 through 5 found by Lanneau and Thiffeault [25]. For genus 2 and 3, the equivalent integer labeled graphs are also given (see Remark 2.11). We use the convention that a filled in vertex is given the sign label '+1' while the unfilled vertex is given the sign label '-1'.

Let δ_g^+ be the minimum dilatation for an orientable pseudo-Anosov mapping class on a closed surface. The minimum orientable examples for genus $g = 2, 4, 5$ can be realized as the closures of classical Coxeter mapping classes associated to bipartite graphs constructed in [38] [27]. For genus 4 and genus 5, the graphs are the classical hyperbolic extensions of the E_7 and E_8 graphs, and in the genus 5 example, the dilatation is equal to Lehmer's number. The hyperbolic extension of E_6

genus	mixed-sign Coxeter graph
2	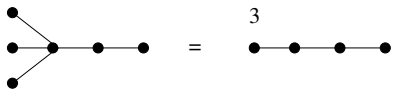
3	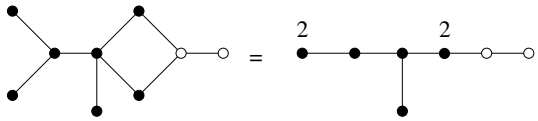
4	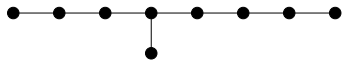
5	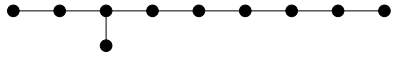

Table 1: Graphs corresponding to minimum dilatation orientable examples for $g = 2, 3, 4, 5$

is given in Figure 8. It's corresponding mapping class is defined on a surface of genus 4, but it has the same dilatation as the genus 3 example given in Table 1.

The sequence δ_g^+ converges to 1. Moreover, we have

$$\log(\delta_g^+) \asymp \frac{1}{g}$$

(see [18]). Thus, classical Coxeter mapping classes cannot realize small dilatation orientable mapping classes for high genus.

Remark 2.22 One can also study dilatations of pseudo-Anosov mapping classes (S, ϕ) in terms of the topological Euler characteristic $\chi(S)$. This is well-motivated by the following. Given a pseudo-Anosov mapping class (S, ϕ), let

$$L(S, \phi) = \lambda(\phi)^{|\chi(S)|}$$

be the *χ-normalized dilatation* of (S, ϕ). Let M be a hyperbolic 3-manifold, and F a fibered face (see [37]). Then F is a polyhedron of dimension equal to $b_1(M) - 1$ where $b_1(M)$ is the first Betti number of M. The rational points in the interior of F correspond to mapping classes (S, ϕ) that are monodromies of fibrations of M over the circle.

On any compact subset of the interior of a fibered face F the χ-normalized dilatation extends to a continuous convex function on F (see [14] [28]) and hence is bounded. Given a pseudo-Anosov (S, ϕ), let (S^0, ϕ^0) be the mapping class obtained by letting $S^0 = S \setminus \mathrm{Sing}(\phi)$, and $\phi^0 = \phi|_{S^0}$. Then (S^0, ϕ^0) is pseudo-Anosov, and $\lambda(\phi^0) = \lambda(\phi)$ (see, Lemma 2.16).

Farb, Leininger and Margalit Universal Finiteness Theorem [11] implies that the collection of mapping classes (S, ϕ) with bounded *χ-normalized dilatation* correspond (after puncturing S at singularities) to rational points on compact subsets of a finite collection fibered faces.

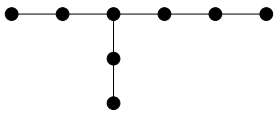

Figure 8: A positive Coxeter graph related to genus 3 example.

As an example, numerically d_3^+ equals the house of the hyperbolic extension of E_6 (see [29], Table 5, and Figure 8). Let (S_{hE_6}, ϕ_{hE_6}) be the mapping class obtained from hE_6 using the bipartite ordering. Then S_{hE_6} has genus 4 and 2 boundary components. The genus 3 example obtained from the graph Γ_3 in Table 1 has 4 boundary components. Thus, the surfaces S_{hE_6} and S_{Γ_3} have the same topological Euler characteristic.

The above discussion suggests another version of the minimum dilatation problem.

Problem 2.23 *Find the minimum dilatation of pseudo-Anosov mapping classes with no interior singularities with a given topological Euler characteristic.*

3 Twist graphs and twisted Coxeter mapping classes

In this section, we define (full) twist graphs, and associated (full) twist mapping classes and use them to prove Theorem 1.7. Twist graphs are elementary building blocks that can be used to construct small dilatation pseudo-Anosov mapping classes via Murasugi sum. We will construct sequences of mapping classes associated to iterative joins of twist graphs, and investigate conditions under which the normalized dilatations are bounded.

Before defining twist graphs and twist mapping classes, we define Murasugi sum for a pair fibered 3-manifolds (Section 3.1). As as example, we recall the definition of Hopf-plumbing for fibered knot and link complements (Section 3.2).

3.1 Generalized Murasugi sums of mapping classes.

The Murasugi sum was originally defined for fibered links in S^3 [30]. In this section we study properties of Murasugi sums for arbitrary mapping classes.

Let P_{2k} be a $2k$-sided polygon with alternate edges removed. The polygon P_{2k} is *properly embedded* in a compact surface S if the boundary components of P_{2k} are contained in the boundary of S, and the interior of P_{2k} is contained in the interior of S.

Let (S_0, ϕ_0) and (S_1, ϕ_1) be two mapping classes with proper embeddings of P_{2k}. Let S be the surface obtained by gluing S_0 and S_1 by identifying the interiors of the embedding of P_{2k} in S_0 to the interior of the embedding of P_{2k} in S_1 after rotating by $\frac{2\pi}{k}$.

Note that the intersection of the closure of $S \setminus S_i$ with S_i is contained in the boundary of S_i for $i = 0, 1$. Thus, we can extend $\phi_i : S_i \to S_i$ by the identity on $S \setminus S_i$ and let $\phi : S \to S$ be the composition $\phi = \phi_1 \circ \phi_0$. The mapping class (S, ϕ) is called the *Murasugi sum* of (S_0, ϕ_0) and (S_1, ϕ_1) relative to the embeddings of P_{2k}.

Murasugi sum and mapping tori. Let M_0 and M_1 be the mapping tori of (S_0, ϕ_0) and (S_1, ϕ_1). Identify S_i with a fiber of M_i. Let $M_i^\diamondsuit$ be the result of cutting M_i along $\iota_i(P_{2k}) \subset S_i$, creating a boundary component homeomorphic to a sphere with hemispheres identified with two copies $\iota_i(P_{2k}^+)$ and $\iota_i(P_{2k}^-)$ of P_{2k} glued together along their boundaries. Let M' be the result of gluing $M_0^\diamondsuit$ with $M_1^\diamondsuit$ along boundary spheres, so that $\iota_0(P_{2k}^+)$ is glued to $\iota_1(P_{2k}^-)$ and $\iota_0(P_{2k}^-)$ is glued to $\iota_1(P_{2k}^+)$.

Lemma 3.1 *The mapping torus M of (S, ϕ) is homeomorphic to M'.*

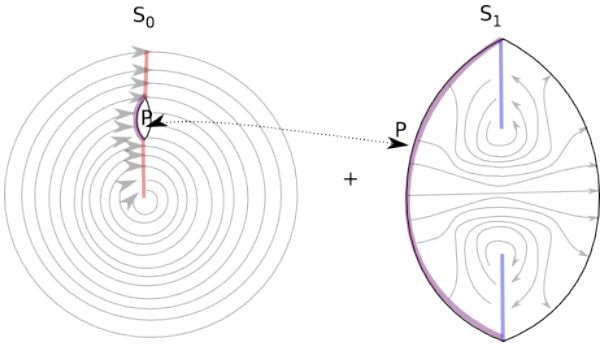

Figure 9: Murasugi sum of surface flows.

To prove Lemma 3.1 it is useful to view the mapping torus of a mapping class (S, ϕ) as a manifold with a continuous surjection

$$\mathfrak{f} : S \times [0, 1] \to M$$

such that

(i) $\mathfrak{f}$ is an embedding on $S \times [1, 0)$, and

(ii) $\mathfrak{f}(s, 1) = (\phi(s), 0)$, for $s \in S$.

An f satisfying (i) and (ii) is called a *surface flow*, with *transverse surface* S identified with $\mathfrak{f}(S \times \{0\})$, and *monodromy* (S, ϕ).

Lemma 3.2 *The map from fibrations to surface flows given by modding out the product $S \times [0, 1]$ by the equivalence $(x, 1) \sim (\phi(x), 0)$ is a bijection.*

Proof. Given a surface flow with transverse surface S and monodromy (S, ϕ), there is corresponding fibration of M over S^1 with monodromy (S, ϕ) defined by contracting the embedded surfaces $\mathfrak{f}(S \times \{t\})$. □

We relax the definition of surface flow slightly to include the following. Let $f : S \times [0,1] \to M$ be a continuous surjective map so that (i) is replaced by

(ia) $\mathfrak{f}|_{(S\times\{t\})}$ is 1-1 for all $t \in [0,1]$; and

(ib) $f(s,t) = f(s',t')$ only if $s = s'$ and for all $t_1 \in [t,t']$, $f(s,t_1) = f(s,t)$.

Given a flow f satisfying $(ia), (ib)$ and (ii), one can continuously deform f until it satisfies (i) and (ii), and hence f determines a unique fibration of M with fiber S. We will use this weaker version of surface flow in what follows.

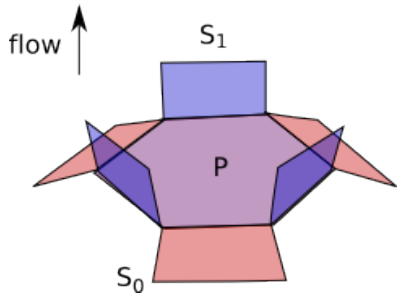

Figure 10: Local gluing of S_0 and S_1 at P with upward surface flow.

Proof of Lemma 3.1. Let $P = P_{2k}$, and let $(M_i, S_i, \mathfrak{f}_i)$ be two flows defined (up to isotopy) by (S_i, ϕ_i), for $i = 0, 1.$. Define a flow $(M, S, \mathfrak{f})$ by $\mathfrak{f} : S \times [0,1] \to M$, where

$$f(s,t) = \begin{cases} \mathfrak{f}_0(s,2t) & \text{if } s \in S_0,\ 0 \le t \le 1/2 \\ \mathfrak{f}_1(s,0) & \text{if } s \in S_1 \setminus \iota_1(P),\ 0 \le t \le 1/2 \\ \mathfrak{f}_0(s,1) & \text{if } s \in S_0 \setminus \iota_0(P),\ 1/2 \le t \le 1 \\ \mathfrak{f}_1(s,2t-1) & \text{if } s \in S_1,\ 1/2 \le t \le 1 \end{cases}$$

The sum of the flows is illustrated in Figure 9. The monodromy ϕ is the isotopy type of the composition $f_1 \circ f_0$. Figure 10 illustrates the local gluing of S_0 and S_1. The map f defines a unique surface flow on M up to isotopy, and hence a fibration of

$$M \to S^1,$$

with monodromy equal to the Murasugi sum of $(S_0, \phi_0$ and (S_1, ϕ_1). □

Example 3.3 Let $\Gamma_i = (\mathcal{V}_i, \mathcal{E}_i)$, $i = 0, 1$ be two mixed-sign Coxeter graphs, and let $v_i \in \mathcal{V}_i$ be fixed vertices. Then the *join* of Γ_0 and Γ_1 at v_0 and v_1 is the graph obtained by taking the disjoint union of Γ_0 and Γ_1 and adding a new edge ϵ between v_0 and v_1. If Γ_0 and Γ_1 are ordered and have fatgraph structure at their vertices, then the *join* is determined by the choice of element $w_i \in \mathcal{V}_{v_i}$ for each $i = 1, 2$. Then v_1 is inserted into $\mathcal{V}_{v_2}$ after w_2, and similarly v_2 is inserted into $\mathcal{V}_{v_1}$ after w_1.

Assume that Γ_i are simply-laced Coxeter graphs with global orderings and local fatgraph structure, let $\mathfrak{s}_i$, $i = 0, 1$ be sign labels on $\mathcal{V}_i$, and let $(S_{\Gamma_i,\mathfrak{s}_i}, \phi_{\Gamma_i,\mathfrak{s}_i})$ be the corresponding Coxeter mapping

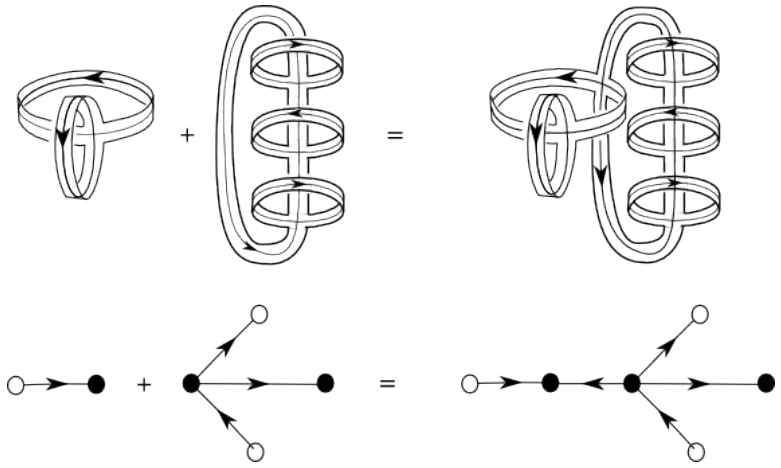

Figure 11: Join of graphs, and corresponding geometric realization.

class. Then for any choice of pairs of adjacent edges at v_0 and v_1, we have a new mixed-sign Coxeter graph with global and local fatgraph structure $(\Gamma, \mathfrak{s})$, and the Coxeter mapping class $(S_{\Gamma,\mathfrak{s}}, \phi_{\Gamma,\mathfrak{s}})$ is obtained from $(S_{\Gamma_i}, \mathfrak{s}_i)$ by Murasugi sum along square a P_4.

Figure 11 shows an example. Although the graphs are drawn with sign-labelings, the geometric realizations only depend on the underlying ordered fatgraphs.

3.2 Hopf plumbing for fibered links

Since the disk is a fiber surface for the complement of the unknot, any sequence of Hopf-plumbings starting with the unknot gives rise to a new fibered 3-manifold. Furthermore, the monodromy is simply the composition of the old monodromy with the monodromy of the Hopf link, that is a right Dehn twist if the twist is clockwise, and a left Dehn twist if the twist is counter-clockwise.

In many cases the mixed-sign Coxeter mapping classes are the monodromy of fibered knots and links in S^3. For example, if we take a configuration of oriented chords $\ell_1, \ldots, \ell_k$ on an oriented disk in S^3 such that the algebraic intersections $\iota_{\text{alg}}(\ell_i, \ell_j) > 0$ for $i > j$, then we can construct a surface $S_{\Gamma,\mathfrak{s}} \subset S^3$ for any choice of labeling $\mathfrak{s}$ as follows. For $i = 1, \ldots, k$, we successively attach a band with a coutner-clockwise (resp., clockwise) full-twist along each chord ℓ_i according to whether $\mathfrak{s}(i)$ is positive (resp., negative). This construction was studied in the positive case ($\mathfrak{s} \equiv 1$) in [16].

Proposition 3.4 *The link complement $S^3 \setminus \partial S_{\Gamma,\mathfrak{s}}$ fibers over the circle with fiber $S_{\Gamma,\mathfrak{s}}$ and monodromy $(S_\Gamma, \phi_{\Gamma,\mathfrak{s}})$.*

Proof. By construction, the link $K = \partial S_{\Gamma,\mathfrak{s}}$ is obtained by a sequence of Hopf-plumbings starting with the disk. Thus, $S^3 \setminus K$ is fibered with fiber $S_{\Gamma,\mathfrak{s}}$.

To find the monodromy, we need only verify that a clockwise twisted Hopf band has monodromy

equal to a right Dehn twist. This is shown in Figure 12. □

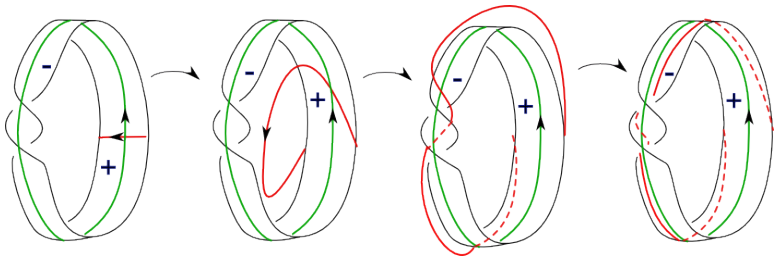

Figure 12: The monodromy of a counter-clockwise twisted Hopf band.

Seifert matrices. Later in this paper, it will be useful to write down the homological dilatation matrix for the monodromy of a fibered link complement.

Let $K \subset S^3$, and let S be a surface embedded in S^3 with $K = \partial S$. Let $x_1, \ldots, x_k$ be a system of simple closed curves on S that generate $H_1(S : \mathbb{Z})$. We can find a matrix representing the action of the monodromy of the fibration as follows (see [32]). For each $i = 1, \ldots, k$, let x_i^+ be the result of pushing x_i into $S^3 \setminus S$ in the positive direction. Let A be the $k \times k$ matrix whose i, j entry is given by the linking number $\ell k(x_i^+, x_j)$.

Proposition 3.5 *The linear map $\phi_* : H_1(S; \mathbb{Q}) \to H_1(S; \mathbb{Q})$ induced by the monodromy (S, ϕ) is defined by the matrix*

$$\phi_* : (A^{tr})^{-1} A.$$

The matrix $(A^{\mathrm{tr}})^{-1}A$ is sometimes known as the Seifert matrix for the spanning surface S.

3.3 Fibered faces and dilatations.

Thurston's fibered face theory for 3-manifolds provides a way to parameterize mapping classes with related dynamics. Let M be an oriented 3-manifold. An element of $\alpha \in H^1(M; \mathbb{Z})$ is *fibered* if the corresponding map $\alpha_* : \pi_1(M) \to \mathbb{Z}$ has finitely generated kernel. By a theorem of Stallings [36], this is equivalent to the existence of a fibration $M \to S^1$ inducing the map α_* on fundamental groups. If α is fibered, let (S_α, ϕ_α) be the *monodromy* of α, that is, $S_\alpha \subset M$ is a general fiber, and $\phi_\alpha : S_\alpha \to S_\alpha$ is the first return map under the flow defined by α.

Thurston defined a norm on $H^1(M; \mathbb{R})$ as follows. For $\alpha \in H^1(M; \mathbb{Z})$, let

$$||\alpha|| = \min\{|\chi(S_\alpha)|\}$$

where S_α ranges over oriented surfaces in S dual to α after removing any connected components of positive Euler characteristic. Thurston showed the following.

Theorem 3.6 (Thurston [37]) *If M is hyperbolic, then $||\ ||$ extends to a norm on $H^1(M; \mathbb{R})$ and the unit ball is a compact convex polyhedron. Furthermore, for every top dimensional open face F*

of the unit ball, either there are no fibered elements in the cone $F \cdot \mathbb{R}^+$ or all the integral points in $F \cdot \mathbb{R}^+$ are fibered with pseudo-Anosov monodromy.

If the cone $F \cdot \mathbb{R}^+$ contains fibered elements, it is called a *fibered cone* and F is a *fibered face*. Given a rational ray from the origin passing through a fibered face F, there is a unique *primitive* integral element α on the ray with relatively prime coordinates. This element α corresponds to a fibration of M over the circle with connected fiber S_α, and for any positive integer k, the element $k\alpha$ corresponds to a fibration of M whose fiber is k copies of S_α. Furthermore, the dilatations of the monodromy ϕ_α and $\phi_{k\alpha}$ are related by

$$\lambda(\phi_{k\alpha}) = \lambda(\phi_\alpha)^{\frac{1}{k}},$$

or

$$\log \lambda(\phi_{k_\alpha}) = \frac{1}{k} \log \lambda(\phi_\alpha).$$

Theorem 3.7 (Fried [14]) *The function*

$$l(\alpha) = \log \lambda(\phi_\alpha)$$

extends to a continuous convex function on each fibered cone $F \cdot \mathbb{R}^+$ that is homogeneous of degree -1 and goes to infinity toward the boundary of F.

Corollary 3.8 *For F a fibered face, and $\alpha \in F \cdot \mathbb{R}^+$, let $\overline{\alpha} = \frac{\alpha}{||\alpha||}$. Then the normalized dilatation function*

$$L(\overline{\alpha}) = \lambda(\phi_\alpha)^{|\chi(S_\alpha)|}$$

defined for integral elements extends to a continuos and convex function on F that goes to infinity toward the boundary of F.

Proof. This follows from the fact that when α is a fibered element $||\alpha|| = |\chi(S_\alpha)|$, where S_α is the fiber of the corresponding fibration of M to S^1. □

Corollary 3.9 *For F a fibered face, and $K \subset F$ an infinite compact subset, the collection of monodromies (S_α, ϕ_α) corresponding to rational points $\overline{\alpha} \in K$ has unbounded topological Euler characteristic and bounded normalized dilatation. In particular, if $\overline{\alpha}_n$ is a sequence of distinct rational points on F converging to an interior element in F, then the corresponding monodromies (S_n, ϕ_n) have unbounded normalized dilatations and bounded normalized dilatation.*

3.4 Full twist braids and their monodromy.

In this section, we define twist maps and twist graphs, and use them as building blocks for constructing sequences of mixed-sign Coxeter mapping classes. The twist maps $(\Sigma_m^{(k)}, R_m^{(k)})$, $m \geq 2$, $k \geq 1$, have the following properties:

1. $(\Sigma_m^{(k)}, R_m^{(k)})$ is the Coxeter mapping class associated to a graph with $\mathfrak{s} \equiv -1$;
2. $(R_m^{(k)})^{km}$ is a product of left Dehn twists on the boundary components of Σ_m;
3. the mapping class $R_m^{(k)}$ preserves a flat structure on $\Sigma_m^{(k)}$ with a distinguished periodic orbit O of order m; and
4. the mapping tori of the restrictions $(\Sigma_m^{(k)} \setminus \mathrm{O}, R_m^{(k)}|_{\Sigma_m^{(k)} \setminus \mathrm{O}})$ are independent of k, and are homeomorphic to the complement of a tubular neighborhood of the link in S^3 drawn in Figure 14.

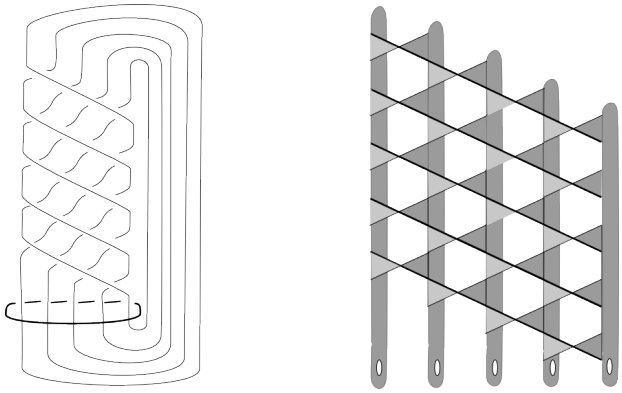

Figure 13: Closure of a full twist braid on 5 strands, and a fiber surface.

Let $b_m^{(k)}$ be the product of k full twist braids on m strands. The corresponding encircled link $L_m^{(k)} \cup E$, where E is the encircling link, is drawn in Figure 13 in the case $m = 5$ and $k = 1$.

Lemma 3.10 *The link complement $S^3 \setminus L_m^{(k)} \cup E$ is independent of k.*

Proof. The complement of a tubular neigborhood $L_m^{(k)} \cup E$ in S^3 is homeomorphic to the complement of the link drawn in Figure 14 The link complement for $L_m^{(k)}$ is obtained from the link in Figure 14 by the surgery that contracts the curve $k\ell + m$, where m is the meridian and ℓ is the longitude of the encircling component E. □

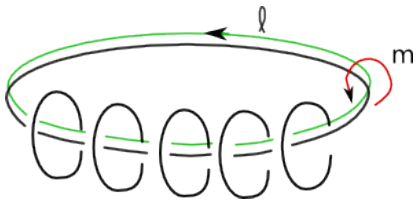

Figure 14: The mapping torus associated to $(\Sigma_m^{(k)}, R_m^{(k)})$.

Consider the fibration of $S^3 \setminus L_m^{(k)} \cup E$ with fiber equal to the surface $\Sigma_m^{(k)}$ drawn on the right in Figure 13. The monodromy is periodic of order km (modulo the action near the boundary), and can be seen explicitly as follows.

The surface $\Sigma_m^{(k)}$ is a union of m *main* disks (drawn vertically in Figure 13) and km *attaching* disks (drawn horirzontally). We can think of the darkly shaded regions as being the positively oriented side of $\Sigma_m^{(k)}$, and the lightly shaded region as being on the negatively oriented side. Number the main disks from right to left $d_1, \ldots, d_m$ and the attaching disks $a_1, \ldots, a_{km}$ from top to bottom. Then the monodromy acts by cyclically permuting the main disks

$$d_1 \to d_2 \to \cdots \to d_m \to d_1$$

while rotating them by $\frac{2\pi}{km}$, and the attaching disks

$$a_1 \to a_2 \to \cdots \to a_{km} \to a_1,$$

while rotating them by $\frac{2\pi}{m}$. The mapping class $R_m^{(k)}$ has the property that $(R_m^{(k)})^m$ rotates the interiors of each of the disks by 360 degrees in the counter-clockwise direction. In other words, it is isotopic to the product of left Dehn twists along boundary parallel curves. Thus we have the following.

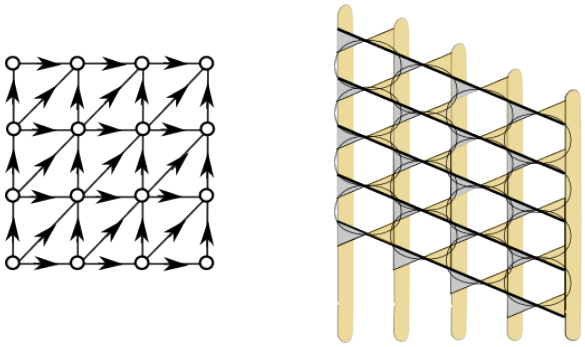

Figure 15: Seifert surface for full twist briad on 5 strands and corresponding Coxeter graph $(T_5^{(1)}, -1)$.

Lemma 3.11 *The twist mapping class* $(\Sigma_m^{(k)}, R_m^{(k)})$ *satisfies*

$$(R_m^{(k)})^{km} = (\partial_1 \circ \partial_2 \circ \cdots \partial_m)^{-1}$$

where ∂_i *is a positive Dehn twist around the* i*th boundary component of* Σ_m*. (Here, the ordering of the* ∂_i *does not matter, since the Dehn twists on the right hand side of the equation commute.)*

We now show that the mapping classes $(\Sigma_m^{(k)}, R_m^{(k)})$ are mixed-sign Coxeter mapping classes.

Consider the graph $T_m^{(k)}$ with $(km-1) \times (m-1)$ vertices shown in the left diagram of Figure 15. This graph captures the combinatorics of the set of loops drawn on the surface $\Sigma_m^{(k)}$ on the right of Figure 15. Order the columns of the graph $T_m^{(k)}$ from left to right, and each column from bottom to top. Starting from the bottom left corner, moving up the first column, then going to the bottom of the second column to the top, etc. This ordering is consistent with arrows in the directed graph shown in Figure 15. Assign the label -1 to all vertices and denote the signed graph by $(T_m^{(k)}, -1)$.

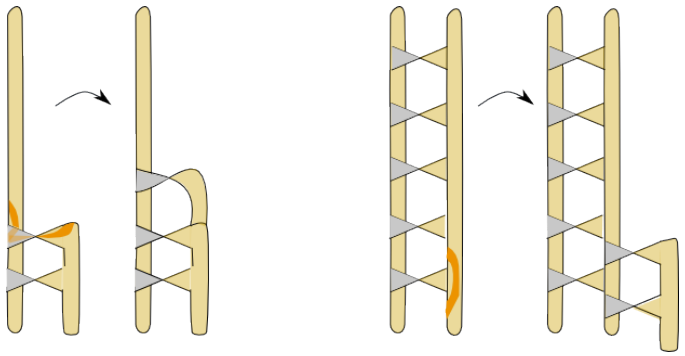

Figure 16: Constructing the embedding of $\Sigma_m^{(k)}$ in S^3 by Hopf plumbings on a disk.

Proposition 3.12 *The monodromy of $S^3 \setminus L_{m,k}$ with fiber $\Sigma_m^{(k)}$ is the mixed-sign Coxeter mapping class associated to the labeled graph $(T_m^{(k)}, -1)$.*

Proof. The surface $\Sigma_m^{(k)} \subset S^3$ is isotopic to the surface obtained by successive Hopf plumbing (see Figure 16). This sequence of clockwise Hopf plumbings is compatible with the ordering on $T_m^{(k)}$. Furthemore, as seen in Figure 17, the Seifert matrix is equal to $-I - A^+(T_m^{(k)})$, where $A^+(T_m^{(k)})$ is the upper triangular part of the adjacency matrix for $T_m^{(k)}$, i.e., the directed adjacency matrix for $T_m^{(k)}$ with the given ordering of vertices. The claim thus follows from Proposition 3.5 and Proposition 2.8. □

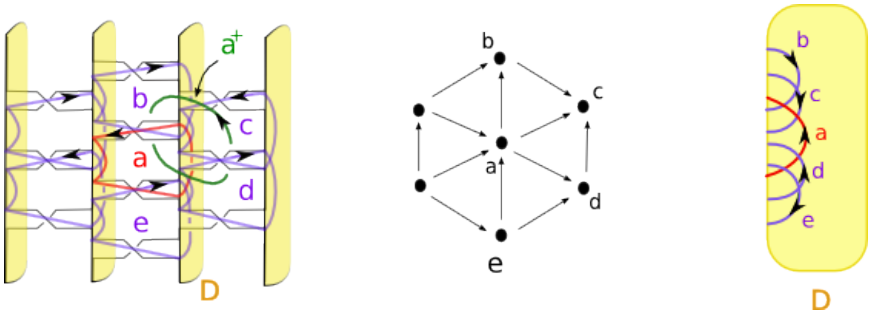

Figure 17: Local picture of $(\Sigma_5^{(1)}, R_m^{(1)})$.

Remark 3.13 A Coxeter system is *spherical* if its associated bilinear form is positive or negative definite, and it is *affine* if its bilinear form is positive or negative semi-definite. In the classical case, where $\mathfrak{s} \equiv 1$, the Coxeter system is spherical or affine if and only if a Coxeter element has spectral radius equal to 1. In the mixed-sign case, the classification problem is more subtle. The graphs $(T_m, -1)$ are examples of mixed-sign Coxeter systems whose Coxeter element has spectral radius one, but is not spherical or affine (for example, the Coxeter group contains hyperbolic elements).

3.5 Flat structure.

We digress in this section by noting that the mapping classes $(\Sigma_m^{(k)}, R_m^{(k)})$ are naturally endowed with a flat structure, Furthermore, $(\Sigma_m(1), R_m^{(1)})$ are translation surfaces. Give each $d_1, \ldots, d_m$ and $a_1, \ldots, a_m$ the flat structure of regular m-gons. Then R_m preserves the induced singular flat structure on Σ_m. More precisely, the m-gons $d_1, \ldots, d_m$, and $a_1, \ldots, a_m$ are each permuted cyclically, preserving centers and rotating the m-gons by an angle of $\frac{\pi}{m}$.

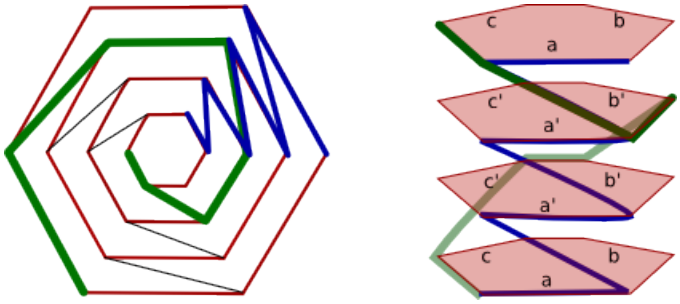

Figure 18: The main disks $d_1, \ldots, d_m, d_{m+1}$, where d_{m+1} is identified with d_1 $(m = 3)$.

Figure 18 shows two views of Σ_m for $m = 3$. The left-most figure shows a view of the surface with boundary, where one of the three boundary curves is drawn spiraling inward. The 3-gons d_1, d_2, d_3 are drawn as hexagons (the innermost hexagon is identified with the outermost hexagon), and the boundary of one of the hexagons a_i is drawn as a zigzag. The right-hand figure gives a side view, where the top hexagon corresponds to the inner hexagon in the left hand diagram. Again the bottom hexagon is identified with the top hexagon. The map R_m takes each d_i and a_i and rotates by an angle of $\frac{\pi}{3}$ in the counter-clockwise direction.

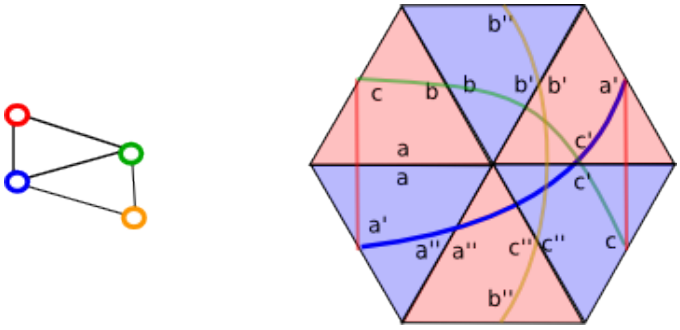

Figure 19: Two views of the twist surface (homeomorphic to a torus) for $m = 3$.

If we shrink the boundary of Σ_m to a point, then the resulting surface can be given a flat structure as the union of $2m$ regular m-gons of equal size. To visualize the flat structure on the closure $\overline{\Sigma}_m$, one contracts the spiraling boundary curves. For example, $\overline{\Sigma}_3$ is a torus, and R_3 preserves its structure as a union of six equilateral triangles. In Figure 19 the surface $\overline{\Sigma}_3$ and its flat structure are shown. Sides labeled with the same symbol are identified. One can see that $\overline{\Sigma}_3$ is a translation surface.

The map R_4 preserves the structure of $\overline{\Sigma}_4$ as the union of 8 squares (Figure 20). Again, we see that $\overline{\Sigma}_4$ is a translation surface. While the flat structure on $\overline{\Sigma}_3$ has no singularities, the flat structure

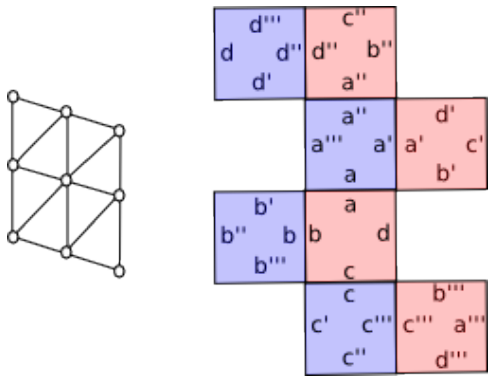

Figure 20: The twist surface for $m = 4$.

on $\overline{\Sigma}_4$ has 4 singularities of degree 2.

3.6 Iterated Murasugi sum with twist maps

In this section we use twist maps $(\Sigma_m^{(k)}, R_m^{(k)})$ to build families of mapping classes with the same mapping torus.

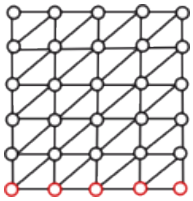

Figure 21: The extended twist graph for $m = 6$.

On the level of Coxeter graphs, the construction goes as follows. Let $(\Gamma, \mathfrak{s})$ be a mixed-sign Coxeter mapping class containing $(A_m, -1)$ as a subgraph, where A_m is the standard spherical Coxeter graph. We define an extended m-twist graph $(\widetilde{T}_m, -1)$ with a distinguished $(A_m, -1)$-subgraph, and define a sequence of graphs $(\Gamma_k, \mathfrak{s}_k)$ obtained by iteratively joining the extended m-twist graphs.

The extended m-twist graph is the graph with $m(m-1)$ vertices shown in Figure 21 for $m = 6$. Figure 22 illustrates the k times iterated m-twist graph $(T_m^k, -1)$ for $k = 3$. This is obtained by identifying the top row of the m-twist graph with the bottom row of the m-twist graph, and repeating.

Now consider a general mixed-sign Coxeter graph $(\Gamma, \mathfrak{s})$ containing an $(A_m, -1)$ subgraph. Let (S_k, ϕ_k) be the mapping class obtained by joining $(\Gamma, \mathfrak{s})$ to the extended $(T_m^{(k)}, -1)$ along $(A_m, -1)$ as in Figure 22.

Lemma 3.14 *The mapping tori for (S_k, ϕ_k), $k \geq 1$, are contained in a single homeomorphism class M of 3-manifolds, and the mapping tori M_k for (S_k, ϕ_k) are Dehn fillings of M along the*

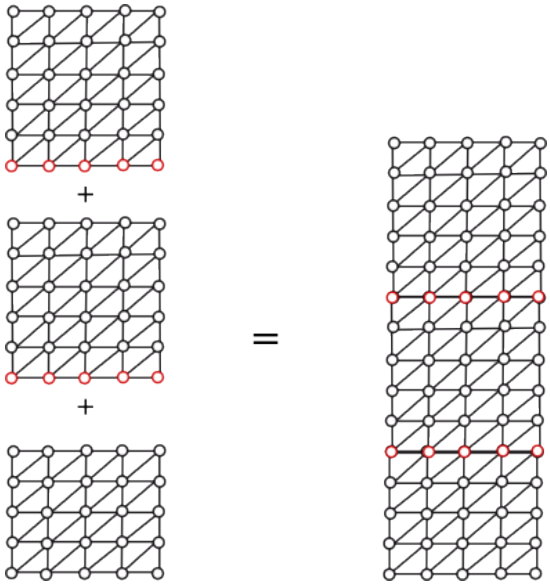

Figure 22: The iterated twist graph (right) for $m = 4$ and $k = 3$.

tubular neighborhood N of the suspension of O, with slope $[1 : k]$ with respect to some fixed choice of generators of $\pi_1(N)$.

Proof. This follows from the fact that the mapping tori for $(\Sigma_m^{(k)}, R_m^{(k)})$ belong to a single homeomorphism class. □

Remark 3.15 The proof above also applies to the iterated Murasugi sum of $(\Sigma_m^{(k)}, R_m^{(k)})$ with an arbitrary mapping class (S, ϕ) containing an embedded P_{2m} whose alternating sides are contained in the boundary of S.

3.7 Attaching tails, and iterated Hopf plumbing.

Consider the special case when $m = 1$. Then the corresponding Coxeter graph is $(A_k, -1)$, where A_k is the classical spherical Coxeter system. In this case, since A_k is a tree, and hence bipartite (see Section 2.5) the signs on the vertices (in this case "-1") can be replaced by 1, and we can take $T_2^{(k)}$ to be the classical A_k diagram.

Let (S, ϕ) is any mapping class with an attaching square, and (S_k, ϕ_k) is the sequence of mapping classes obtained by attaching $(\Sigma_1^{(k)}, R_1^{(k)})$. We call (S_k, ϕ_k) the sequence of mapping classes obtained from (S, ϕ) by *attaching a tail.*

A *Salem-Boyd* sequence of polynomials is a sequence of the form

$$P_k(x) = x^k Q(x) + Q^*(x)$$

where $Q(x)$ is a monic integer polynomial, and $Q^*(x) = x^{\deg(Q)}Q(1/x)$ is the *reciprocal* of $Q(x)$. These sequences were used in [35] and [7] to study properties of Salem numbers. The house $|P_k|$ of P_k has the following properties (see, [16] Theorem 12).

Theorem 3.16 *If $P_k(x) = x^k Q(x) + Q^*(x)$ is a Salem-Boyd sequence, then*

(i) the number of roots of P_k outside the unit circle is monotone increasing, and eventually constant, and

(ii) $\lim_{k\to\infty} |P_k| = |Q_k|$.

Mapping classes (S_k, ϕ_k) corresponding to graphs with tails are studied in [16] in the case when the graph is dual to a chord system on a disk. In this case, it is shown that the mapping classes are the monodromy of a sequence of links L_k in S^3, obtained from a single fibered link L_0 by twisting a suitable pair of strands. Furthermore, the Alexander polynomial, or characteristic polynomial of the action of ϕ_k on first homology, is a Salem-Boyd sequence. The proof (see [16], Theorem 9) relies only on the form of $(\phi_k)_*$ given in Proposition 2.8 and Proposition 2.12.

Theorem 3.17 ([16], Theorem 9) *The Alexander polynomial Δ_k corresponding to (S_k, ϕ_k) is a Salem-Boyd sequence, and hence the homological dilatations $\lambda_{hom}(\phi_k)$ form a convergent sequence.*

Corollary 3.18 *Let (S_k, ϕ_k) be obtained by attaching a single tail to a mapping class (S, ϕ). Then either*

(i) $\lambda_{hom}(\phi_k) = 0$ for all k, or

(ii) $|\Delta_k|$ converges to a real number greater than one.

Proof. This follows from Theorem 3.17 and Theorem 3.16. □

Corollary 3.19 *Let $(\Gamma, \mathfrak{s})$ be a connected mixed-sign Coxeter graph, $v \in \mathcal{V}$ a distinguished vertex, and $(\Gamma_k, \mathfrak{s}_k)$ the join of $\Gamma, \mathfrak{s}$ with $(A_k, \mathfrak{s}(v))$. Let (S_k, ϕ_k) be any Coxeter mapping class associated to $(\Gamma_k, \mathfrak{s}_k)$. Then either*

(i) ϕ_k is periodic,

(ii) ϕ_k is pseudo-Anosov, but $\lambda_{hom}(\phi_k) = 0$ for all k, or

(iii) for large k, ϕ_k is pseudo-Anosov, and there is a constant C such that

$$\lambda(\phi_k) \geq C > 1.$$

Proof. Since Γ is connected, each ϕ_k is either periodic, or ϕ_k is pseudo-Anosov. If $|\Delta_k| > 1$ for some k, then, by Corollary 3.18, $\lambda_{\text{hom}}(\phi_k) = |\Delta_k|$ is greater than one for k large enough. In this case, by Proposition 2.13, ϕ_k is pseudo-Anosov, and, for any $\epsilon > 0$, $\lambda(\phi_k) \geq \ell - \epsilon$, where $\ell = \lim_{k\to\infty} |\Delta_k|$. □

Example 3.20 Let $(\Gamma_{m,n}, \mathfrak{s})$ be the graph in Figure 23. Since $T_1^{(k)}$ is a bipartite graph, and hence (by Theorem 2.17) it is interchangeable with the standard A_n-Coxeter graph with all signs positive. Thus, we can think of this graph as being obtained from the connected two vertex graph with opposite sign labels on the vertices by joining m and n iterated twist graphs of width $r = 1$. Since the graph is bipartite, the ordering of the vertices does not change value of $|\omega_{\Gamma_{m,n},\mathfrak{s}}|$. Let $(S_{m,n}, \phi_{m,n})$ be the mapping class associated to $(\Gamma_{m,n}, \mathfrak{s})$. The surface $S_{m,n}$ has genus

$$g_{m,n} = \left[\frac{m+n}{2}\right],$$

and one or two boundary components, according to whether $m+n$ is even or odd. Here $[a]$ denotes the greatest integer less than or equal to a real number a. In particular, $g_{m,m} = m$.

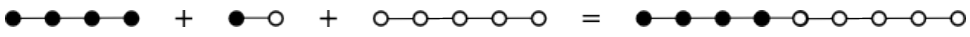

Figure 23: mixed-sign Coxeter graph $(\Gamma_{4,5}, \mathfrak{s})$ obtained by joining twist graphs of width 1.

The mapping classes $(S_{m,n}, \phi_{m,n})$ have also been studied in a different form by P. Brinkmann [8] and [18] (cf. [39]), yielding the following.

Theorem 3.21 (Brinkmann [8], Hironaka-Kin [18], Tsai [39]) *For all m, n, $(S_{m,n}, \phi_{m,n})$ is pseudo-Anosov, and for fixed $m + n$, the dilatation is minimized when $m = n$. Furthermore,*

$$\log(\lambda(\phi_{g,g})) \asymp \frac{\log(g)}{g}.$$

The following question is open.

Question 3.22 *Is there a mixed-sign Coxeter graph $(\Gamma, \mathfrak{s})$ with vertices $v_1, \ldots, v_m$ (possibly counted with multiplicity) so that the mapping classes $(S_{\overline{k}}, \phi_{\overline{k}})$ associated to the joins of $(\Gamma, \mathfrak{s})$ with iterated k_i- twists of width 1 at each of the v_i, $\overline{k} = (k_1, \ldots, k_m)$, has the asymptotic behavior*

$$\log(\lambda(\phi_{\overline{k}})) \asymp \frac{1}{g_{\overline{k}}}, \tag{4}$$

where and $g_{\overline{k}}$ is the genus of $S_{\overline{k}}$?

3.8 Asymptotically small dilatation Coxeter mapping classes.

In this section, we prove Theorem 1.7 by showing the existence of a sequence of mixed-sign Coxeter mapping classes (S_k, ϕ_k) whose closures $(\overline{S}_k, \overline{\phi}_k)$ have the following properties:

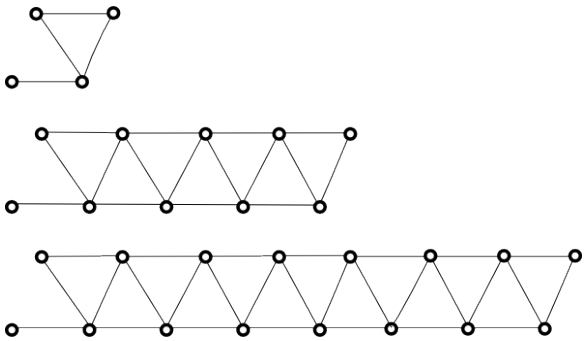

Figure 24: A negatively signed Coxeter fatgraph for $k = 1$, $k = 2$ and $k = 3$.

(i) $\overline{\phi}_k$ is pseudo-Anosov,

(ii) the associated stable and unstable foliations are orientable,

(iii) $\overline{S}_k$ has monotone increasing genus g_k,

(iv) $\lambda(\overline{\phi}_k)$ approaches 1, and furthermore

$$\lim_{k\to\infty} \lambda(\overline{\phi}_k^{g_k}) = \frac{3+\sqrt{5}}{2},$$

the smallest known accumulation point of genus-normalized dilatations.

The mapping classes (S_k, ϕ_k) are obtained from the mixed-sign Coxeter mapping classes corresponding to the negatively signed graphs Γ_k drawn in Figure 24 by closing over all but 3 boundary components. The graphs are given their fatgraph structures as planar graphs.

To show that the mapping classes (S_k, ϕ_k) satisfy the conditions (i)-(iv), we relate them to the monodromy of the links drawn in 25. The figure shows pairs of equivalent link diagrams for the mapping tori of (S_k, ϕ_k), $k = 1, 2$. In the left versions the shaded region shows the contribution of the copies of (Σ_3, R_3). The links beside them on the right shows an equivalent positive braid version of the links. The graphs Γ_k give rise to the Seifert surfaces corresponding to the latter planar projection of the links after closing over suitable boundary components.

Lemma 3.23 *The mapping classes* (S_k, ϕ_k) *corresponding to* $(\Gamma_k, -1)$ *satisfy (i)-(iv).*

By Lemma 3.14, the mapping tori for (S_k^0, ϕ_k^0) belong to a single homeomorphism class, in this case, it is the complement M of the 6_2^2-link L in S^3 (see, the knot table in [32]). The link is shown in Figure 26.

The mapping class, written as $\phi_0 = \sigma_1\sigma_2^{-1}$ in terms of the standard braid generators, is known as the simplest hyperbolic braid monodromy, The fibered face defined by the braid monodromy ϕ_0 shown in the link diagram in Figure 26 was studied in [17]. The link L has two components, K_1 corresponds to the strands of the braid, and K_2 is the encircling link. Let $t \in H_1(M, \mathbb{Z})$ be the meridian loop around K_1 and let $u \in H_1(M; \mathbb{Z})$ be the meridian loop around K_2. Let ξ be the

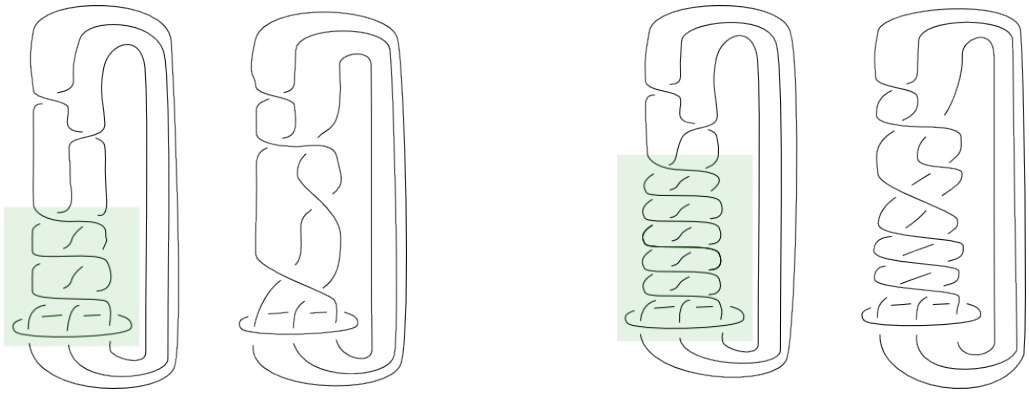

Figure 25: Link diagram for S_k, ϕ_k, for $k = 1, 2$.

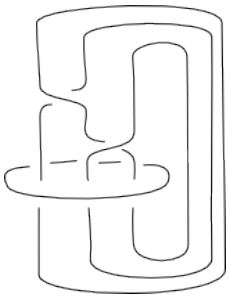

Figure 26: The 6_2^2-link.

dual to t and ψ the dual to u in $H^1(M;\mathbb{Z})$. Then ψ is the fibration of M corresponding to the braid monodromy ϕ_0. Given a fibration $\alpha : M \to S^1$, there is a corresponding element of $H^1(M;\mathbb{Z})$ defined by the induced map $\alpha_* : H_1(M;\mathbb{Z}) \to \mathbb{Z}$, and hence we can write

$$\alpha_* = a\psi + b\xi.$$

The integers a and b are determined by the condition that α_* restricted to $H_1(S_\alpha;\mathbb{Z})$ is trivial, where S_α is any fiber of α.

For each k, we will show that (S_k, ϕ_k) is the monodromy of $6k\psi + \xi$. The link diagrams for (S_k, ϕ_k) can be obtained from that of the 6_2^2-link shown in Figure 26, by removing a tubular neighborhood of K_2, and refilling with meridian μ_2', where

$$\mu_2' = \mu_2 - k\ell_2.$$

Under the induced homomorphisms $\psi_*, \xi_* : H_1(M;\mathbb{Z}) \to H_1(S^1;\mathbb{Z}) = \mathbb{Z},$, we have $\psi_*(\mu_2') = 1$, and $\xi_*(\mu_2') = -3k$. Thus, (S_k, ϕ_k) is the monodromy of the fibration defined by $\psi_k = 3k\psi + \xi$.

The homological and geometric dilatations of (S_k, ϕ_k) can be computed from the Teichmüller and Alexander polynomials of M. Since 6_2^2 is a symmetric braid (that is, if one can move the link isotopically to get the same link diagram with K_1 and K_2 switched) it follows that the fibered face for ψ and invariants like the Teichmüller polynomial are the same as those of the fibered face for ξ (after switching variables). For the 6_2^2-link complement, the Thurson norm is defined by

$$||(a, b)|| = \max\{|2a|, |2b|\},$$

so for $k > 1$, ψ_k lies in the fibered face containing ξ, and the rays through ψ_k in $H^1(M;\mathbb{R})$ converge to the ray through ξ. Using the computations in [28] and [17], we have the following.

Corollary 3.24 *The mapping classes (S_k, ϕ_k) have genus $3k-1$.*

Proposition 3.25 *The homological and geometric dilatations of (S_k, ϕ_k) are given by*

$$\lambda_{geo}(\phi_k) = \lambda(\phi_k) = |LT_{1,3k}| = |x^{6k} - x^{2k+1} - x^{3k} - x^{3k-1} + 1|,$$

and

$$\lambda_{hom}(\phi_k) = |x^{6k} - x^{3k+1} + x^{3k} - x^{3k-1} + 1|.$$

Corollary 3.26 *When k is even, then (S_k, ϕ_k) is orientable, and attains Lanneau and Thiffeault's conjectural minimum dilatation for orientable pseudo-Anosov mapping classes on closed surfaces of even genus.*

Corollary 3.27 *The mapping class (S_2, ϕ_2) is a minimum dilatation orientable mapping class for genus $g = 5$..*

The following was proved (in stronger form) in [17] using fibered face theory.

Lemma 3.28

$$\lim_{k\to\infty} \lambda(\phi_k)^{3k} = \frac{3+\sqrt{5}}{2}.$$

This completes the proof of Theorem 1.7.

References

[1] J. Aaber and N. Dunfield. Closed surface bundles of least volume. *Algebr. Geom. Topology*, 10:2315–2342, 2010.

[2] N. A'Campo. Sur les valeurs propres de la transformation de Coxeter. *Invent. Math.*, 33(1):61–67, 1976.

[3] J. Armstrong. Principal elements of mixed-sign coxeter systems. *Florida State Univeristy, PhD. Thesis*, 2012.

[4] M. Bauer. Examples of pseudo-Anosov homeomorphisms. *Trans. Amer. Math. Soc.*, 330(1):333–359, 1992.

[5] J. Birman. *Braids, links, and mapping class groups.* Number 82 in Annals of Math. Studies. Princeton University Press, Princeton, NJ, 1974.

[6] N. Bourbaki. *Groupes et algèbres de Lie*. Hermann, Paris, 1968.

[7] D.W. Boyd. Small Salem numbers. *Duke Math. J.*, 44(2):315–328, 1977.

[8] P. Brinkmann. A note on pseudo-Anosov maps with small growth rate. *Experimental Math.*, 13(1):49–53, 2004.

[9] J. Cho and J. Ham. The minimal dilatation of a genus two surface. *Experiment. Math.*, 17:257–267, 2008.

[10] I. Dolgachev. Reflection groups in algebraic geometry. *Bull. of the A.M.S.*, 45(1):1–60, 2008.

[11] B. Farb, C. Leininger, and D. Margalit. Small dilatation pseudo-anosovs and 3-manifolds. *Adv. Math*, 228(3):1466–1502, 2011.

[12] B. Farb and D. Margalit. *A Primer on Mapping Class Groups*. Princeton University Press, 2011.

[13] A. Fathi, F. Laudenbach, and V. Poénaru. Some dynamics of pseudo-Anosov diffeomorphisms. In *Travaux de Thurston sur les surfaces*, volume 66-67 of *Astérisque*. Soc. Math. France, Paris, 1979.

[14] D. Fried. Flow equivalence, hyperbolic systems and a new zeta function for flows. *Comment. Math. Helvetici*, 57:237–259, 1982.

[15] J-Y Ham and W. T. Song. The minimum dilatation of pseudo-Anosov 5-braids. *Experimental Mathematics*, 16(2):167,180, 2007.

[16] E. Hironaka. Chord diagrams and Coxeter links. *J. London Math. Soc.*, 69(2):243–257, 2004.

[17] E. Hironaka. Small dilatation pseudo-Anosov mapping classes coming from the simplest hyperbolic braid. *Algebr. Geom. Topol.*, 10:2041–2060, 2010.

[18] E. Hironaka and E. Kin. A family of pseudo-Anosov braids with small dilatation. *Algebr. Geom. Topol.*, 6:699–738, 2006.

[19] F. Hirzebruch. Über Singularitäten komplexer flächen. *Rend. Math. Appl.*, pages 213–232, 1966.

[20] R. Howlett. Coxeter groups and M-matrices. *Bull. London Math. Soc.*, 14(2):137–141, 1982.

[21] J. Humphreys. *Reflection groups and Coxeter groups*. Cambridge University Press, Cambridge, 1990.

[22] E. Kin and M. Takasawa. Pseudo-anosovs on closed surfaces having small entropy and the whitehead sister link exterior. *J. Math. Soc. Japan*, 65(2):411–446, 2013.

[23] K.H. Ko, J.E. Los, and W.T. Song. Entropies of braids. *J. of Knot Theory and its Ramifications*, 11(4):647–666, 2002.

[24] C. Labruère and L. Paris. Presentations for the punctured mapping class groups in terms of Artin groups. *Algebr. Geom. Topol.*, 1:73–114, 2001.

[25] E. Lanneau and J.-L. Thiffeault. On the minimum dilatation of pseudo-Anosov homeomorphisms on surfaces of small genus. *Ann. de l'Inst. Four.*, 61(1):164–182, 2009.

[26] E. Lanneau and J.-L. Thiffeault. On the minimum dilatation of braids on the punctured disc. *Geom. Dedicata.*, 152(1):165–182, 2011.

[27] C. Leininger. On groups generated by two positive multi-twists: Teichmuller curves and Lehmer's number. *Geometry & Topology*, 88:1301–1359, 2004.

[28] C. McMullen. Polynomial invariants for fibered 3-manifolds and Teichmüller geodesics for foliations. *Ann. Sci. École Norm. Sup.*, 33:519–560, 2000.

[29] C. McMullen. Coxeter groups, Salem numbers and the Hilbert metric. *Publ. Math. Inst. Hautes Études Sci.*, 95:151–183, 2002.

[30] K. Murasugi. On the genus of the alternating knot. i,ii. *J. Math.Soc. Japan*, 104:94–105,235–248, 1958.

[31] R. Penner. Bounds on least dilatations. *Proceedings of the A.M.S.*, 113(2):443–450, 1991.

[32] D. Rolfsen. *Knots and Links*. Publish or Perish, Inc, Berkeley, 1976.

[33] E. Rykken. Expanding factors for pseudo-Anosov homeomorphisms. *Michigan Math. J.*, 46(2):281–296, 1999.

[34] K. Saito. Around the theory of the generalized weight system: relations with singularity theory the generalized weyl group and its invariant theory, etc. *Amer. Math. Soc. Transl. (2)*, 183:101–143, 1998.

[35] R. Salem. A remarkable class of algebraic integers. proof of a conjecture of vijayaraghavan. *Duke Math. J.*, 11:103–108, 1944.

[36] J. Stallings. Constructions of fibered knots and links. *Proc. Symp. Pure Math.*, 27:315–319, 1975.

[37] W. Thurston. A norm for the homology of 3-manifolds. *Mem. Amer. Math. Soc.*, 339:99–130, 1986.

[38] W. Thurston. On the geometry and dynamics of diffeomorphisms of surfaces. *Bull. Amer. Math. Soc. (N.S.)*, 19(2):417–431, 1988.

[39] C. Tsai. The aymptotic behavior of least pseudo-Anosov dilatations. *Geometry and Topology*, 13:2253–2278, 2009.

[40] O.V. Lyashko V. I. Arnold, V.V. Goryunov and V.A.Vasil'ev. *Singularity Theory I.* Springer-Verlag, Berlin, 1991.

[41] A. Valdivia. Sequences of pseudo-Anosov mapping classes and their asymptotic behavior. *New York J. Math.*, 18, 2012.